Check for updates

Chemical representation learning for toxicity prediction†‡

Jannis Born, [ID] §*[ab] Greta Markert, [ID] §[ac] Nikita Janakarajan, [ID] [ad] Talia B. Kimber, [ID] [e] Andrea Volkamer, [ID] [ef] María Rodríguez Martínez¶[a] and Matteo Manica [ID] ¶[a]

Undesired toxicity is a major hindrance to drug discovery and largely responsible for high attrition rates in early stages. This calls for new, reliable, and interpretable molecular property prediction models that help prioritize compounds and thus reduce the high costs for development and the risk to humans, animals, and the environment. Here, we propose an interpretable chemical language model that combines attention with multiscale convolutions and relies on data augmentation. We first benchmark various molecular representations (*e.g.*, fingerprints, different flavors of SMILES and SELFIES, as well as graph and graph kernel methods) revealing that SMILES coupled with augmentation overall yields the best performance. Despite its simplicity, our model is then shown to outperform existing approaches across a wide range of molecular property prediction tasks, including but not limited to toxicity. Moreover, the attention weights of the model allow for easy interpretation and show enrichment of known toxicophores even without explicit supervision. To introduce a notion of model reliability, we propose and combine two simple methods for uncertainty estimation (Monte-Carlo dropout and test-time-augmentation). These methods not only identify samples with high prediction uncertainty, but also allow formation of implicit model ensembles that improve accuracy. Last, we validate our model on a large-scale proprietary toxicity dataset and find that it outperforms previous work while giving similar insights into revealing cytotoxic substructures.

1 Introduction

The costs of research and development per new FDA-approved drug have been doubling every 9 years since 1950.[1] A major bottleneck in this process is toxicity which is alone responsible for the failure of >30% of all clinical trials.[2] A commonly utilized approach in lead compound design is to avoid molecules with toxicophores, *i.e.*, substructures or chemical motifs that are likely to exert toxic effects.[3] Alternatively, computational approaches can be used for tasks such as activity prediction in order to design more active and selective compounds.[4] Empirically, these heuristics have proven to be limited—the success rates are steadily declining and oncological pharmaceuticals are particularly affected as only 3.4% of the clinical trials are successful.[5] Even worse, oncology drugs in clinical trials often do not work by their proposed mechanism of action. Lin A. *et al.*[6] found that when knocking out the target genes of 10 cancer drugs in clinical trials, all 10 drugs retained their efficacy through other

mechanisms, suggesting that off-target toxicity is a common mechanism of action of anticancer drugs in clinical trials.

Therefore, more precise computational approaches that help reduce the costs of development and the risks posed to humans and the environment throughout the process are desired. Machine learning (ML) methods have been applied in the field of quantitative structure–activity relationship (QSAR) prediction for decades.[7,8] Lately, deep learning (DL) has promised a methodological turnaround toward data-driven approaches to combat the ever-growing need for new therapeutics[9] and in some instances, replaced ML methods.[10] Consequently, a considerable body of literature developed around molecular property and activity prediction[11–15] with several studies focusing on toxicity prediction.[16–21] It is widely accepted that the choice of the selected molecular representation for model building plays a crucial role in accurately predicting small molecule properties and bioactivities.[22] Traditional chemoinformatics typically relied on 1D descriptors such as binary fingerprints;[23] however in the past few

[a]IBM Research Europe, Zurich, Switzerland. E-mail: jab@zurich.ibm.com

[b]Department of Biosystems Science and Engineering, ETH Zürich, Switzerland

[c]Department of Chemistry and Applied Biosciences, ETH Zürich, Switzerland

[d]Department of Computer Science, ETH Zürich, Switzerland

[e]In silico Toxicology and Structural Bioinformatics, Institute of Physiology, Charité-Universitätsmedizin Berlin, Charitéplatz 1, 10117, Berlin, Germany

[f]Data Driven Drug Design, Saarland University, 66123 Saarbrücken, Germany

years, chemical language models relying on the molecular inline notation SMILES[24] have gained popularity for QSAR prediction models.[22,25,26] But despite the ubiquitous usage of SMILES, there is no universal, canonical SMILES representation (*e.g.* `PubChem` kekulizes "canonical" SMILES, whereas `RDKit` does not), even though several attempts toward unification have been proposed.[27]

In this work, we systematically investigate the predictive power of models built on different flavors of SMILES and compare it to established chemical descriptors such as molecular fingerprints or more complex representations such as graphs. We propose a novel, uncertainty-aware and interpretable chemical language model. While this model has been developed mainly in the context of toxicity prediction, it is a generic molecular property prediction model that, as we demonstrate, exhibits excellent prediction performance across several datasets, focused on but not limited to toxicity.

Model interpretability is a heavily sought-after trait in QSAR modeling since most DL models are black-boxes. Considerable previous work has been invested to explain molecular property prediction models[28] and contributions of individual parts of a molecule to its properties or effect.[29,30] However, unlike previous work[31,32] our model does not require any post-hoc workflow such as integrated gradients which itself suffers from limitations such as gradient saturation[32] to become interpretable. Instead, we achieve high model explainability *via* a built-in-attention mechanism.[33] This is an *ante hoc* interpretability method that produces attention maps as a byproduct of a prediction. Building upon our previous work[26] where we demonstrated the utility of the attention mechanism in a regression task (drug sensitivity prediction) by reporting that (1) highly attended genes significantly enrich apoptotic processes and (2) molecular attention correlates strongly with similarity of functional fingerprints, we herein show how attention maps can be useful to understand the model's predictive process and find that the attention maps align, in many cases, with prior knowledge about toxicophores. Since model safety and reliability is a critical aspect of drug modeling, we borrow two simple uncertainty estimation methods proposed in related fields[34,35] and provide quantitative evidence on how they can be used to identify probable misclassifications. Compared to graph-based models,[13,36] our method is significantly simpler and solely relies on the SMILES chemical language. It exploits data augmentation – through the non-uniqueness of SMILES - to boost model performance and outperforms previous studies on this task.

2 Methods

2.1 Problem formulation

Let $\mathcal{M}$ denote the molecular space and $\mathcal{Y}$ denote the QSAR property scores, *e.g.* measured toxicity of a molecule. We are interested in learning a function $\Phi: \mathcal{M} \rightarrow \mathcal{Y}$ that maps a molecule to a property score. The function Φ is learned from a labelled dataset $\mathcal{D} = \{m_i, y_i\}_{i=1}^{N}$ where $m_i \in \mathcal{M}$ and $y_i \in \mathcal{Y}$.

2.2 Molecular representations

Throughout this work we compare three classes of molecular representations:

(1) Molecular fingerprints: molecular fingerprints are binary 1D vectors where the value at each position indicates the presence (or absence) of a certain substructure. Here, we use extended connectivity fingerprints (ECFPs[23]), that are based on the Morgan algorithm[37] as a baseline. We use ECFP4, the most common choice in the literature,[38] with 512 bits.

(2) Molecular graphs: each molecule is denoted by an undirected graph $G = (V, E)$ where atoms denote vertices and bonds denote edges. Vertices are labelled with their atom identity (chemical element) and edges by the bond order (*e.g.* a single or double bond).

(3) String-based representations: we examine molecular inline notations, namely SMILES[24] and SELFIES.[39] Due to their recent success in QSAR prediction models[26] and even epitope-related tasks,[40] different types of string representations, in particular different SMILES flavors, are our main focus.

2.2.1 SMILES flavors. SMILES (simplified molecular input line entry specification) was introduced by Weininger D.[24] and is a molecular inline notation that is obtained by traversing the molecular graph. One special feature of the SMILES notation is that a valid SMILES string is possible starting from whichever atom in the molecule. Typically, SMILES strings do not explicitly list bonds such as single bonds (-) or aromatic bonds (:), unless they are double ($=$) or triple (#). In a kekulized format (typically used by RDKit), capital letters represent non-aromatic atoms, whereas small letters represent aromatic ones. In a non-kekulized format (typically used by PubChem), aromatic atoms are not explicit, as they are represented by capital letters connected through alternating single and double bonds. Numbers are used to denote rings. One can think of it as an imaginary cut between bonds of two neighboring atoms in a ring. The ring-closing number occurs twice: once for the atom that "opens" the ring and once for the atom that "closes" it (*e.g.*, cyclohexane is represented as `C1CCCCC1`; it is important to notice that the first `C1` and the second `C1` are not representing the same atom). Branches, *i.e.*, when an atom has three or more bonds, are represented using parentheses. Hydrogen atoms are also not stated explicitly except if they are important for the stereo information of a tetrahedral center (*e.g.*, `[C@H]`). Stereoisomers have the same atomic sequence and the same molecular formula, but differ in the three-dimensional orientation of their atoms which can lead to different behaviours in chiral environments (*e.g.*, enzymes). Stereoisomers used as drugs can have huge differences in toxicity and potencies.[41] For the description of stereoisomers in SMILES, one considers the first token before the token containing `@` or `@@` as the chiral centre. The remaining atoms connected to the central atom are listed either by ordering them anticlockwise (`@`) or clockwise (`@@`). The choice whether to use clockwise or anticlockwise notation is arbitrary (*e.g.*, `C[C@H](O)C=C` is equivalent to `C[C@@H](C=C)(O)`). Generally, there are 2^n possible stereoisomers, where n is the number of stereo centers. As a consequence, if the stereoinformation is removed from a molecule with two stereocenters, the SMILES string is ambiguous and could represent four different molecules. This is exemplarily depicted in Fig. A2, see ESI.‡ The same holds true for molecules with information about the bond direction ($\backslash \ldots /$ or $/ \ldots \backslash$ for

(S,E)-4-phenylbut-3-en-2-ol

Example molecule and its different SMILES representations:
Raw: SMILES as read from data source: `c1ccc(/C=C/[C@H](C)O)cc1`

Chemical transformations
Canonical (by `RDKit`): `C[C@H](O)/C=C/c1ccccc1`
Isomeric (by `PubChem`): `C[C@@H](/C=C/C1=CC=CC=C1)O`
Without stereoinformation: `c1ccc(C=CC(C)O)cc1`
Without chirality: `c1ccc(/C=C/C(C)O)cc1`
Remove doublebond direction: `c1ccc(C=C[C@H](C)O)cc1`
Kekulization: `C1=CC=C(/C=C/[C@H](C)O)C=C1`
Explicit bonds: `c1:c:c:c(/C=C/[C@H](-C)-O):c:c1`
Explicit hydrogens: `[cH]1[cH][cH][c](/[CH]=[CH]/[C@H]([CH3])[OH])...`

Randomized transformations (non-unique!)
Multiplicity (aka augmentation) – e.g.: `C[C@H](O)C=Cc1ccccc1`
Character shuffling – e.g.: `c[C@H]Ccc/C(Cc=Oc)1/)c(`

Language translation
SELFIES: `[C][C@H1][Branch1][C][O][C][=C][C][=C][C]...`

Tokenization
If SMILES:
Character level: `C [ C @ H ] ( O ) C = C c 1 c c c c c 1`
Atom-level: `C [C@H] ( O ) C = C c 1 c c c c c 1`
SMILES Pair Encoding (SPE): `C[C@H](O) /C=C/ c1ccccc1`
If SELFIES:
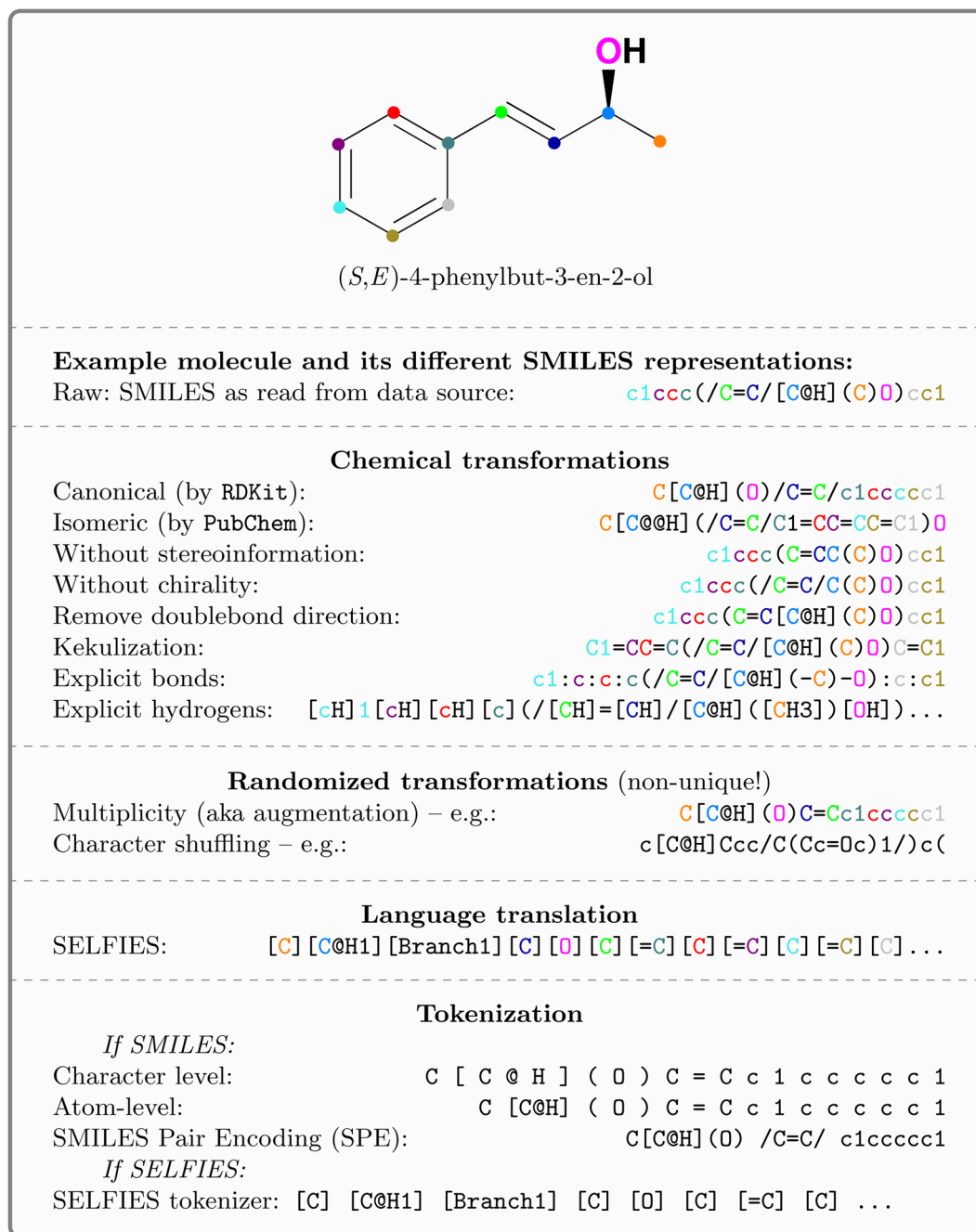SELFIES tokenizer: `[C] [C@H1] [Branch1] [C] [O] [C] [=C] [C] ...`

Fig. 1 Explored SMILES flavors, exemplified on (S,E)-4-phenylbut-3-en-2-ol. Transforming a molecule into a string representation can be divided into four transformation groups which are executed sequentially. For visual clarity and to pronounce the relation between the SMILES sequence and the depiction, atoms are colored.

(E), respectively, and $\backslash...\backslash$ or $/.../$ for (Z), respectively. Here, the removal of the information about the bond direction can have greater consequences, as the SMILES string can represent molecules with very different molecular properties (again 2^n, where n represents the number of explicit bond directions in the molecule). Fig. 1 gives an overview of the explored SMILES flavors. The starting point is always the raw SMILES representation as read from the data source.

Chemical transformations refer to semantic changes in the visibility of certain properties in the string and include:

(1) Canonicalization: since a molecular graph traversal is non-univocal, usually, traversed graphs start at a non-hydrogen atom and proceed in any user-defined direction. Therefore, SMILESs are non-unique representations of molecules. Canonicalization ensures that every molecule is represented by exactly one string. Here, we use canonicalization as defined in `RDKit`.[42] Canonicalization has the advantage of increased data uniformity.

(2) Kekulization: aromatic moieties can either be represented explicitly or implicitly. In the explicit (kekulized) version,

the aromatic π-electrons are static between every second carbon. Instead, in the canonical form, the electrons are delocalized (*cf.* Fig. 1). The kekulized version is slightly longer but uses the same token to denote an atom, irrespective of its aromaticity.

(3) Removal of stereoinformation: to uniquely identify a molecule from a SMILES, information about the tetrahedral center or the double bond direction (*E* or *Z*) is sometimes needed. Since stereoinformation is not always explicitly denoted in datasets, it is often discarded in affected molecules for reasons of simplicity and uniformity. We experiment separately with removing chirality and bond direction. Once removed, the SMILES string is ambiguous and can represent different molecules (*cf.* Fig. A2, see ESI‡).

(4) Explicitness: we experimented with making hydrogen atoms or single bonds (or both) explicit in the SMILES. This not only increased sequence length but also better distributes the frequency of tokens in the vocabulary.

Randomized transformations refer to non-chemical changes in the syntax or grammar of the language. Since they are stochastic, they resemble a form of data augmentation.

(1) Augmentation: since SMILESs are non-unique, their multiplicity can be used for data augmentation and provably improves performance of predictive[15,43] and generative[44] models. Here, we use online augmentation which samples the graph traversal and generates the corresponding string at runtime, similar to random rotations or cropping of images. This makes it impossible to measure the actual inflation of training molecules; however as shown in Fig. A3, see ESI,‡ we empirically report the number of obtained augmentations for all Tox21 molecules. For the majority of molecules more unique SMILES can be obtained than the usual number of training epochs (100); some molecules even showed >100 000 unique SMILESs.

(2) Shuffling: Liu P. *et al.*[45] observed that randomly shuffling the position of the SMILES tokens (*i.e.*, destroying their local structure) does not significantly reduce performance in QSAR prediction tasks. Similar to augmentation, shuffling occurs as a stochastic transformation at runtime.

Language translations are optional. The default language is SMILES and the only alternative language explored in this work is SELFIES.

(1) SELFIES: SELFIES is a self-referencing chemical language that overcomes the validity problem of SMILES (*i.e.*, random SMILES strings are not generally valid) and was devised for generative models.[39]

Note that most of the transformations can be combined (see appendix Fig. A1, see ESI‡ for a flowchart about their combination). The entire SMILES processing pipeline is implemented in the publicly available package `pytoda`.‖[46]

Tokenization: lastly, the obtained strings are split into tokens to ensure that each molecular entity (*e.g.*, the atom `Br`) is represented as one feature vector to the model. SMILESs are split with the regular expression from Schwaller P.[47] As an alternative tokenization method, we explored SMILES pair

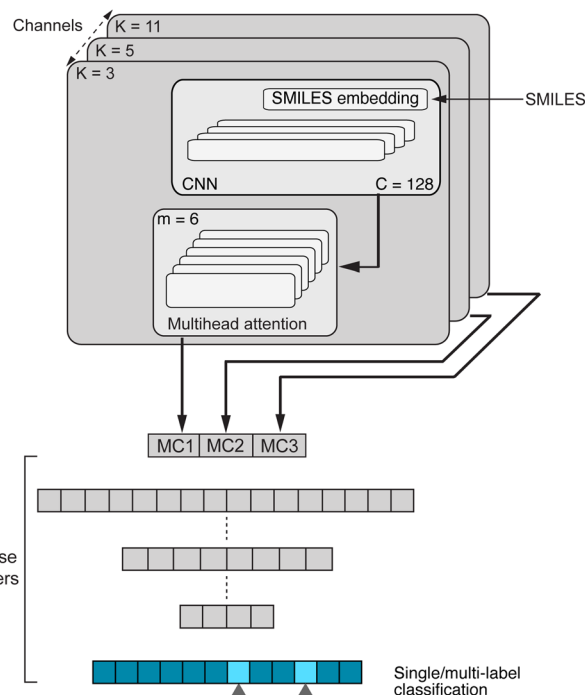‖ https://pypi.org/project/pytoda

Fig. 2 Our CLM, a convolutional, attention-based neural network for molecular property prediction. The first step is sequence embedding which is then used for three (parallel) 1D convolutional layers to aggregate local information. Next, the multi-head-attention mechanism calculates the attention weights and filters the inputs accordingly. The resulting outputs of all three multiscale convolutional (MC) blocks as well as one residual connection (not shown) are concatenated and processed by a set of dense layers, resulting in one (or multiple) output scores. *C* denotes the number of convolutional filters and *m* is the number of attention heads.

encodings (SPEs), a method inspired by byte-pair encodings that splits SMILES into substructures of varying lengths based on their occurrence in ChEMBL.[48] They showed that SPE exhibits prediction accuracy comparable to that of atom-based tokenization in QSAR prediction tasks.[48] SPE is ideal to handle larger molecules since it drastically reduces the number of tokens. For example, the SMILES shown in Fig. 1 is split into "`c 1 c c c ( / C = C / [C@H] ( C ) O ) c c 1`" whereas SPE splits into "`c1ccc( /C=C/ [C@H](C) O)cc1`". In our experiments, we coupled the SMILES PE tokenizer with SMILES augmentation. For SELFIES, the split function built in the `SELFIES` package is used. All sequences are enclosed by `<START>` and `<STOP>` tokens and are left-padded to the longest sequence in the dataset, respectively.

2.3 Models

2.3.1 String-based models

Chemical language model (CLM). Our proposed CLM model is an attention-based multiscale convolutional neural network. It is inspired by a bimodal variant of this model, called `PaccMann`, which was originally developed for drug sensitivity prediction[26,49] but has also inspired proteochemometric models for binding affinity prediction.[50,51] The network architecture is

shown in Fig. 2. In our canonical CLM, each token is represented as a learned embedding of dimensionality $H = 256$, such that the input matrix $\mathbf{X} \in \mathbb{R}^{T \times H}$ where T is the sequence length (*i.e.*, padding size). Note that we performed ablation studies on the embedding type. The embeddings $\mathbf{X}$ are processed by three parallel 1D-convolutional layers with kernel sizes 3, 5, and 11. A fourth channel has a residual connection without convolutions (not shown in Fig. 2). For each of the four channels, we utilize a stack of $m = 6$ attention heads. In each head, an attention mechanism, similar to the one proposed by Bahdanau, D.[33] and developed prior to the one by ref. 52 is used to enable the model to focus on relevant parts of the molecule. In each head, the attention weight α_i of token i is computed using:

$$\alpha_i = \frac{\exp(u_i)}{\sum_j^T \exp(u_j)}, \text{ where } \vec{u} = (MW_1)\vec{v} \tag{1}$$

where $\mathbf{M} \in \mathbb{R}^{T \times C}$ is the output of the convolutional layer with $C = 128$ filters, $W_1 \in \mathbb{R}^{C \times A}$ and $\vec{v} \in \mathbb{R}A$ are learnable parameters, and $A = 256$ is the dimensionality of the attention space. For notational purposes, $\mathbf{A} = [\vec{\alpha}, ..., \vec{\alpha}] \in \mathbb{R}T \times C$ should be considered the attention matrix with the attention vector repeated C times. Then, the output vector $\mathbf{e} \rightarrow \in \mathbb{R}C$ of each attention head is obtained by filtering $\mathbf{M}$ with the attention matrix (*i.e.*, "we attend"):

$$\vec{x}_{\text{out}} = \mathbf{1}^{\text{T}}[\mathbf{M} \circ \mathbf{A}] \tag{2}$$

Basically, we filter the output sequence from a given convolutional kernel with the attention scores and then we sum over the sequence dimension to obtain a single score for each filter. This is similar to the attention by ref. 33 with the difference that (1) we refrain from having an additional tan h nonlinearity (it did not perform well in initial experiments) and (2) there is no need for additive attention because there are no output tokens to attend to. With three parallel convolutional layers (plus one residual connection), each with m attention heads, we obtain $4m$ output vectors $\vec{x}_{\text{out}}$ which are stacked to form a single large vector and processed by a stack of dense layers ([1024, 512] units) before a final layer with a sigmoid activation computes the class-wise predictions. The model is trained with a binary cross-entropy loss.

Recurrent networks. We examined two flavours of recurrent neural networks; the gated recurrent unit, GRU,[53] and the neuromodulated bistable recurrent cell, nBRC.[54] The GRU employs a gating mechanism to control the information flow, making it suitable for handling longer sequences. The nBRC is a biologically inspired modification of the GRU that is superior to the other cells in exact memorization and counting,[54] crucial properties when handling SMILES sequences due to the presence of ring opening and closure symbols. The cell can switch between a monostable and a bistable state and can hold onto information for an arbitrarily long period of time. For both models, we use two bidirectional layers with 256 units. The last hidden states from both directions are processed by a 3-layered dense network with 1024, 1024, and 512 hidden units respectively (50% dropout). The final scores are returned by an

ensemble of 5 linear networks acting on the 512-dimensional representation. The models were optimized by Adam[55] at a constant learning rate of $1e - 4$.

2.3.2 Fingerprint-based models. For fingerprint-based models we used 512-bit ECFP fingerprints[23] with a radius of 2 (ECFP4). Additionally, we increased the bit size of the fingerprints to 1024 and 2048 for experiments with the random forest model.

Random forests. Random forests[56] are popular non-linear models that show competitive performances on most classification tasks.[56,57] Owing to high class imbalance in the data, the class_weight parameter was set to balanced. We also performed hyperparameter optimisation on the number of trees in the forest and found 500 to be optimal in line with prior work.[58,59]

k-nearest-neighbor (k-NN). As a non-parametric baseline, we explored the *k*-NN algorithm and employed (inverted) Tanimoto similarity[60] as a distance function. We set $k = 23$, based on the performance on the Tox21 *test* dataset (see subsection 2.6.1).

Dense neural network (DNN). This was a simple, four-layered, fully connected neural network with 512, 1024, 2048, and 1024 units with a sigmoid activation function.

2.3.3 Graph-based models. Molecular graph representations were examined with graph neural networks and graph kernels.

Graph convolutional network (GCN). Following Duvenaud D. K. *et al.*,[61] a GCN with two graph-convolutional layers (64 units) and one dense layer (128 units), no dropout, 75 atom features, and a sigmoid activation function was employed.

Graph kernels. Graph kernels rely on a kernel $k(x,x')$ that measures similarity between molecular graphs x and x'.[62] We experimented with four different kernels.

(1) Shortest-path (SP): this path kernel[63] first transforms the graphs G_1 and G_2 into shortest-path graphs S_1 and S_2 using the Floyd algorithm.[64] Let $S_1 = (V_1, E_1)$ and $S_2 = (V_2, E_2)$, then our shortest-path kernel is:

$$k_{\text{shortest-paths}}(S_1, S_2) = \sum_{e_1 \in E_1} \sum_{e_2 \in E_2} k_{\text{walk}}^{(1)}(e_1, e_2) \tag{3}$$

where $k^{(i)}$ walk is a positive definite kernel on edge walks of length 1.

(2) Weisfeiler–Lehman (WL): This subtree kernel relies on the Weisfeiler–Lehman (WL) relabeling method.[65] Let $G_n = (V, E, l_n)$ and $G'_n = (V', E', l'_n)$ be the n-th iteration rewriting of the graphs G and G'. Then the WL kernel is defined as

$$k_{\text{WL}}^{\text{h}}(G, G') = \sum_{n=0}^{h} k_\delta\left(G_n, G'_n\right) \tag{4}$$

where

$$k_\delta\left((V, E, l), (V', E', l')\right) = \sum_{v=V} \sum_{v \in V'} \delta\left(l(v), l'(v')\right) \tag{5}$$

where δ is the Dirac kernel.

(3) Message passing (MP): this subtree kernel[66] extends the concept of message-passing[67] from GNNs to graph kernels. It's a generalization of the WL kernel that uses a smoother definition of structural equivalence.

(4) Wasserstein-Weisfeiler Lehmen (WWL): this extension of the WL kernel relies on the Wasserstein distance between node

feature vector distributions of the WL subgraphs. For details see Togninalli M. *et al.*[68]

In all cases, the graph kernels were used to measure sample similarity and a support vector machine (SVM)[69] was employed for classification.

2.4 Attention analysis

As a byproduct of the forward-pass, our CLM produces attention scores assigning relevance to each token. We analysed the attention to assess whether the attention scores carry any meaning regarding the toxicity of the respective token (*i.e.*, atom/bond). Therefore, we relied on so-called toxicophores, molecular substructures that are known to have toxic effects.[70] Dependent on the dataset, specific toxicity alerts were employed (see details in the respective results section) and training molecules were excluded from the analysis. The attention scores were computed following eqn (1) which provides a single attention score α_i for each token of the (SMILES) sequence. Atom and bond tokens were considered for the analysis whereas attention on other tokens (*e.g.*, ring tokens) was discarded since it could not always be determined whether these tokens belong to a toxicophore or not. Next, all analyzed molecules (given in SMILES) were queried against the desired toxicity alerts (given in the SMARTS pattern[71]). Whenever a match was obtained (by a substructure match in `RDKit`), the SMILES tokens affected by the alert were assigned as toxicophore tokens whereas the other tokens kept their non-toxic status. This resulted in a grouping of the attention weights as either belonging to a toxic or non-toxic substructure.

2.5 Uncertainty estimation

In an attempt to obtain a trustworthy model, we further employ two techniques to measure prediction uncertainty. Specifically, we assess epistemic (model) uncertainty with Monte Carlo dropout (MC dropout), a method that draws Monte Carlo samples from the approximate predictive posterior by performing repeated forward passes of an input sample while the network's dropout layers are turned on.[34] Moreover, we assess aleatoric (data) uncertainty, an uncertainty measure independent of epistemic uncertainty, *via* test-time data augmentation.[35] In our case, this amounted to performing repeated forward passes with different SMILES strings corresponding to the same molecule.[43]

From the resulting prediction ensembles, the confidence estimate c_i of sample i was obtained by scaling the sample's standard deviation to the range [0,1] and interpreting it as inverse precision:

$$c_i = -\left(\frac{\sigma_i - \sigma_{\min}}{\sigma_{\max} - \sigma_{\min}}\right) + 1, \tag{6}$$

where σ_i is the sample standard deviation of the prediction ensemble, $\sigma_{\min}$ is the minimal standard deviation (0, *i.e.*, all predictions are identical) and $\sigma_{\max}$ is the maximal standard deviation (0.5, *i.e.*, 50% of the predictions are 0 and 50% are 1). The above procedure is identical to the one we described in ref. 49. We further propose to use μ_i, the sample mean of the prediction ensemble, as an alternative prediction and show that it yields improved performance. In practice, 200 forward

passes were performed for both methods. The dropout value was 0.5.

2.6 Datasets

2.6.1 Tox21 dataset. In 2014, the US-EPA initiated a data challenge called "Toxicology in the 21st Century" (Tox21). In the context of this challenge, a database was produced, that includes 12 707 compound entries of small molecules tested on 12 targets.[72,73] The input data are binarily classified as toxic or non-toxic.

Five of the 12 targets are associated with hormones (such as the estrogen receptor (ER and the ER ligand binding domain), the androgen receptor (AR and the AR ligand binding domain), and aromatase). Both receptors, the ER and AR, regulate gene expression and are important in sexual maturation and gestation.[74] Aromatase catalyzes the hormone reaction from testosterone to estradiol. Aromatase deficiency can lead to delayed puberty in females, osteoporosis in males and virilisation in pregnant mothers. Excess leads to the contrary: premature puberty and breast evolution in males.[75] The other seven belong to stress response pathways (HSE, MMP, ATAD5, PPARγ, ARE, AhR, and p53). Cells activate the heat shock factor response element (HSE) in response to stressful conditions. The mitochondrial membrane potential (MMP) decreases during apoptotic cell death.[76] A low ATPase family AAA domain containing 5 (ATAD5) expression leads to an extended lifespan which leads to an increase of inactive replication factories resulting in a delay in S-phase progression.[77] Peroxisome proliferator-activated receptor γ (PPARγ) plays a major regulatory role in energy homeostasis.[78] The antioxidant responsive element (ARE) regulates cytoprotective genes, which play a critical role in redox homeostasis.[79] In addition to regulating metabolizing enzymes through gene expression, the aryl hydrocarbon receptor (AhR) has roles in regulating immunity, stem cell maintenance, and cellular differentiation. The induction of metabolizing enzymes can lead to the production of toxic metabolites.[80]

When cells undergo DNA damage, the tumor-suppressor protein p53 is expressed, in order to counteract the effects. It induces growth arrest, repairs the DNA or starts the cell death process.[81] However, it is also linked to drug resistance in cancer cells.[82]

The dataset comes with a fixed split of 11 764 *training*, 296 *test*, and 647 *score* molecules. Test labels were withheld from participants during the original Tox21-challenge but later made available so that participants could refine their models for the final evaluation on the molecules in the *score* set.

2.6.2 MoleculeNet datasets. The MoleculeNet benchmark[11] distributes a variety of molecular classification datasets from quantum mechanics over physical chemistry and biophysics to physiology. All datasets use binary but potentially multilabel classifications.

(1) BACE: this is a dataset of 1522 inhibitors against human β-secretase 1 (BACE-1), represented quantitatively by their IC_{50} values and qualitatively through binary labels indicating their inhibition success.[83] The 2D structures of these compounds and IC_{50} values are gathered from the experimental scientific

literature. Scaffold splitting is recommended for this dataset. This dataset has only one task.

(2). SIDER: Side Effect Resource (SIDER) is a database of 1427 approved drugs and their associated adverse drug reactions (ADR), grouped into 27 tasks (*i.e.*, system organ classes[84,85]).

(3) ClinTox: this dataset comprises 1491 drug compounds and holds drugs approved by the FDA as well as those that have failed clinical trials due to toxicity. This dataset has two tasks: clinical trial toxicity status and FDA drug approval status.[86,87]

(4) BBBP: the blood–brain barrier penetration (BBBP) dataset contains information on the blood–brain barrier permeability properties of over 2000 compounds.[88] This is a single binary classification and a scaffold split is recommended.

(5) HIV: the HIV dataset contains information about the ability of 40 000 compounds to block HIV replication.[89] This single binary classification task categorizes compounds as being active or inactive for HIV replication. A scaffold split is recommended.

(6) Tox21: this is a redistribution of the original Tox21 dataset.[90] While there are still 12 tasks there are several important differences that are detailed below. A random split is recommended.

On each dataset, we trained ten models on repeated data splits according to the recommended strategy. For a comparison with Grover,[13] who trained the models on scaffold splits for all datasets, we additionally trained ten models on scaffold splits for the affected datasets (SIDER, ClinTox, Tox21).

Difference between original Tox21 and MoleculeNet Tox21. Like all other datasets from the MoleculeNet that are distributed *via* DeepChem,[91] their Tox21 dataset does not come with a fixed split, and thus, by convention, repeated splits with different random seeds are performed. The DeepChem distribution is significantly smaller, containing only 8014 molecules (SMILESs are largely canonicalized). A detailed analysis of the differences is available in Table A1, see ESI.‡ We believe that these differences are important to emphasize as they have been confounded/disregarded in some prior work.

2.6.3 Cytotoxicity dataset. As an external validation, a cytotoxicity dataset compiled by the Leibniz-Forschungsinstitut für Molekulare Pharmakologie (FMP) was employed.[92] The data collected by the FMP measure the cytotoxicity of molecules and were initially used in a study by Webel, H. E. *et al.*[30] The relative growth of two cell lines, namely HEK292 (kidney) and HepG2 (liver), is measured. A compound is considered cytotoxic if it inhibits growth by at least 50% in at least one of the two cell lines. The data set before pre-processing consists of 34 848 measured compounds. Pre-processing of the data is performed in the same manner as in the original study.[30] More specifically, it uses `RDKit` and consists of a sanitization, a standardization, and a de-duplication step, resulting in 34 366 compounds. Out of these molecules, only 4.65% are labeled cytotoxic, leading to a highly imbalanced, yet consistent, data set. The experiments with this data set were run using high-performance computer (HPC) services from the Freie Universität Berlin.[93] To compare to the feed-forward neural network (FNN) by Webel H. E. *et al.*,[30] we used a 10-fold stratified cross-validation split with 10% held-out data for testing, as performed in their work. Note that Webel H. E. *et al.*[30] used 2048-bit ECFP4s.

2.7 Hyperparameter optimization

All models were trained for 200 epochs with early stopping, the Adam optimizer,[55] and a cross-entropy loss. The learning rate varied across models, but unless otherwise specified, was set to $1e-4$.

Emulating the original Tox21 challenge, the hyperparameters of the models were tuned using the test dataset using raw SMILESs as inputs. After the optimal configuration was found, 10 models were trained for each investigated dataset. For the original Tox21 dataset, the 10 models were obtained from identical training data with different weight initializations. For the remaining datasets, the random split was repeated for each run. Note that we refrained from further optimizing any hyperparameters on any of the remaining datasets.

2.8 Performance metrics

All models were evaluated on performance metrics that are in alignment with previous work on those datasets.[11,30,90] The main metric is the area under the ROC curve (ROC-AUC). For the cytotoxicity dataset, we report the true positive rate (TPR, also called sensitivity), the true negative rate (TNR, also called specificity), and the balanced accuracy $\left(\dfrac{\text{TPR} + \text{TNR}}{2}\right)$.

3 Results

In the following, we will first examine the impact of using different types of property prediction models as well molecular representations on the Tox21 dataset. Then, we will pick the best model and deepen our analysis by comparing it to a large body of related work on several datasets from the MoleculeNet benchmark. We will demonstrate the interpretability of our method by analzying the attention scores – a natural byproduct of every prediction – and also propose two simple uncertainty estimation techniques that improve robustness as well as model performance. Last, we show in a case-study how our CLM can be applied to a proprietary, large-scale dataset and achieve improved performance in virtual screening.

3.1 Model & data representation comparison on Tox21

In Table 1, we display the performance of the different algorithms and representations as measured using ROC-AUC. The performances refer to the Tox21 score dataset which was used to determine the Tox21 challenge winners. Comparing the model classes shows that graph kernels generally yielded the worst performance. Since the complexity of graph kernels scales quadratically with the size of the dataset, reports on graph kernels on datasets with >10 000 examples are scarce to absent.[94] Thus, graph kernels are predominantly useful in small data regimes. The random forests, on the other hand, prove to be a strong baseline, second only to the GCN (0.828 ROC-AUC). We see that increasing the fingerprint bit-size improves the performance of the RF with an ROC-AUC score of 0.782 for the higher 1024-bit and 2048-bit ECFP4s. This suggests that while the random forest requires more information about the molecule to achieve higher classification accuracy, it saturates

Table 1 ROC-AUC values on the Tox21 dataset for different algorithms and molecular representations. All neural network simulations were repeated 10 times. Across all representations and models, the best ROC-AUC values were obtained with augmented SMILES and the CLM architecture (marked in bold). TOP: Different molecular string notations used to train the proposed CLM. Models denoted with a star are significantly outperformed by the best model (augmented SMILES, $p < 0.05$, U). BOTTOM: Overview of the remaining model architectures and molecular representations. All models were significantly inferior to the CLM model with augmented SMILES ($p < 0.05$, U)

Representation	ROC-AUC
Raw SMILES	$0.832* \pm 0.005$
Canonical SMILES	$0.830* \pm 0.008$
Kekulized SMILES	$0.830* \pm 0.006$
Augmented SMILES	**0.853 ± 0.003**
SMILES without bond direction	$0.834* \pm 0.006$
SMILES without chirality	$0.834* \pm 0.004$
SMILES w/o bond direction & chirality	$0.835* \pm 0.006$
Kekulized w/o bond direction & chirality	$0.831* \pm 0.004$
SMILES with explicit bonds	$0.834* \pm 0.003$
SMILES with explicit hydrogen	$0.829* \pm 0.007$
SELFIES	$0.827* \pm 0.007$
Augmented SELFIES	*0.852 ± 0.004*
Shuffled SMILES	$0.830* \pm 0.003$
SMILES pair encoding	$0.776* \pm 0.01$
Augmented SMILES pair encoding	$0.825* \pm 0.005$

Model	Repr.	ROC-AUC
Random forest (RF)	512-bit ECFP4	0.774 ± 0.002
	1024-bit ECFP4	0.782 ± 0.002
	2048-bit ECFP4	0.782 ± 0.002
KNN	512-bit ECFP4	0.759
DNN	512-bit ECFP4	0.777 ± 0.004
GRU (RNN)	Raw SMILES	0.781 ± 0.003
nBRC (RNN)	Raw SMILES	0.756 ± 0.002
Weisfeiler lehman (WL)	Graph kernels	0.754 ± 0.019
Message passing		0.703 ± 0.040
Wasserstein-WL		0.758 ± 0.023
Shortest path		0.567 ± 0.108
GCN	Graphs	0.828 ± 0.008

beyond a certain point when there is no new information to be gained.

The SMILES representations used to train the CLM (*cf.* Table 1) yielded a performance that statistically significantly surpassed (one-sided Mann–Whitney U test, U) the DNN trained on ECFP as well as all graph kernel techniques in all cases. By comparing the SMILES representations, it was found that the best results were not obtained by consistently formatting the SMILES, but rather by SMILES augmentation,[43] which resembles a form of data augmentation by exploiting the multiplicity of SMILES for each molecule. This SMILES augmentation model outperforms all other models ($p < 1e - 4$, U) that do not use augmentation. This is in alignment with prior work reporting superiority of SMILES augmentation to canonical SMILES.[15,43] Generally, the differences between different SMILES representations were minor. Stereochemistry information stemming from chirality tokens (/ and \) or bond direction ([C@H])

tend to confuse the model as removing them yielded slightly better performance, which maybe explainable by their scarcity in the training data (18% and 7% respectively). Notably, even though SELFIESs were devised for generative tasks,[39] they barely rank behind SMILES regarding their predictive power for toxicity prediction. A previously unreported finding is that the benefits of SMILES augmentation also extend to SELFIES. While, overall, the semantic (*i.e.*, chemical) transformation of SMILES has a minor impact on performance, language transformations and the tokenization scheme can be critical. For example, SMILES pair-encoding[48] gave a much worse performance than all other SMILES representations, maybe because the sequences are shorter and the vocabulary is much larger leading to sparsity. We hypothesize that more labelled data or pretraining on SMILES-PE could have closed this gap. A staggering finding is that shuffling the SMILES did not change the performance significantly. This result is in accordance with ref. 45 on other datasets and suggests that instead of aggregating local information in the SMILES sequences, the models predominantly make predictions similar to a bag-of-words model. If structural information is stripped off, the models can only rely on atom counts. However, the shuffling can be interpreted as another form of data augmentation since it is performed stochastically at runtime. In that sense, it is worth mentioning that the SMILES augmentation performed significantly better than shuffling. Last, the two RNN-based models operating on raw SMILES (GRU and nBRC) performed much worse than the CLM, suggesting the superiority of our architecture.

While we used learned embeddings throughout all experiments in this section, we conducted an ablation study comparing them to one-hot embeddings and pretrained embeddings from a variational autoencoder trained on >2M ChEMBL molecules.[46] In the absence of augmentation, the pretrained embeddings significantly outperform the one-hot and especially the learned embeddings. As can be seen in Table A2, see ESI,‡ this holds especially true if the pretrained embeddings are allowed to be finetuned. The use of augmentation consistently improved performance across all embedding types and generally relaxed differences between embedding types.

Since this section demonstrated the superiority of (1) the use of SMILES augmentation, all remaining results are generated with this configuration.

3.2 Analysing attention scores in light of toxicophores

Our proposed CLM utilizes an attention mechanism (similar to the one proposed by Bahdanau D. *et al.*[33]) which naturally returns attention maps indicating relevance for each SMILES token. In contrast to the work by ref. 32, our method cannot provide signed attributions for each atom. However, as the attention scores are a natural byproduct of the forward pass, no postprocessing scheme (*e.g.*, integrated gradients) has to be applied. In our previous work, a predecessor of this attention mechanism demonstrated positive quantitative evidence (for the extraction of genes related to apoptotic processes) in a drug
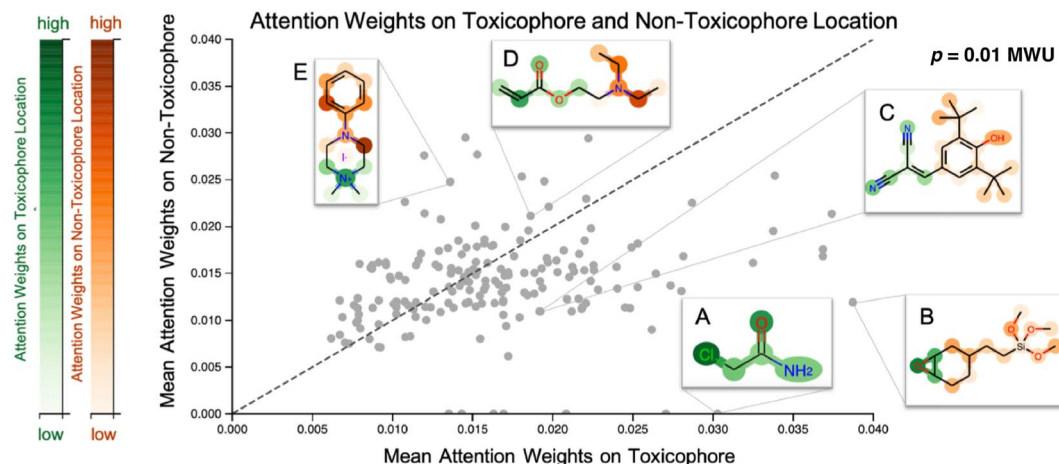
Fig. 3 Visualization of attention maps of Tox21 compounds. Scatterplot of the mean attention of the toxicophore part of the molecule *versus* the mean attention of the remaining ones. Toxicophoric atoms are colored green, the remaining parts are colored red, and intensity encodes the attention weight. Toxicophores are assigned significantly higher attention weights. Interactive visualization is available at: https://ibm.biz/tox21_attention. MWU denotes a Mann−Whitney U test.

sensitivity regression task.[26] We sought to validate the attention scores with toxicophores (molecular substructures with known toxic effects), investigate whether the scores align with known toxicophores, and compare them quantitatively and qualitatively. In Fig. 3, we show the attention weights of the best model for all molecules from the Tox21 score dataset. We focus on two toxicity endpoints, acute aquatic toxicity (99 alerts, see ref. 95 and 96) and endocrine disruption (35 alerts, see ref. 97) that are most similar to the Tox21 tasks. The corresponding SMARTSs were extracted from ref. 98. Similar to the results by Nendza M. *et al.*[97] we found that not all appearances of toxicophores lead to a toxic compound.

To assess whether the model selectively focused on informative substructures, we compared the mean attention weight on the toxicophoric parts of all molecules to the mean attention weight of the remaining part. Molecules that exclusively consisted of toxicophores were excluded from the analysis. This revealed a significantly higher mean for toxicophore substructures ($p = 0.011$ in the two-sided MWU) showing that the model focused predominantly on toxic substructures. This is remarkable given that the attention scores were learned entirely unsupervised. While several related studies on proteochemometric modeling claimed *via* case studies that similar SMILES attention mechanisms could automatically re-discover biochemical concepts such as protein binding sites,[99,100] Li S. *et al.*[101] demonstrated later in a quantitative analysis that performance was not exceeding the chance level. Instead, on the Tox21 dataset previous work by Mayr A *et al.*[16] and Preuer K *et al.*[102] reported that the activation of a significant number of hidden neurons in ECFP-based DNNs could be associated with toxicophore features. However, both their analyses were performed on training molecules and involved significant post-hoc experimentation whereas our attention scores are produced *en passant* the forward pass. Moreover, we emphasize that the attention maps are global, *i.e.*, not assay-specific, and thus, the task-specific inference is limited to single-task classifications. To further assess the usability of

attention maps we enclose a case study where the attention highlighted an epoxide (*cf.* Fig. A5, see ESI‡).

3.3 Comparison to existing QSAR models

We sought to validate the proposed model on related tasks beyond toxicity prediction. The MoleculeNet benchmark[11] is ideally suited for this since it comprises several molecular datasets ranging from biophysical and physiology tasks. To ensure fair comparability, we excluded previous work whenever the data splitting strategy was not clear or no repeated experiments were conducted. The results on all six datasets are shown in Table 2 and underline the superiority of our model to previous approaches, including graph convolutional networks[11] and several variants of message-passing neural networks,[67] in particular, the directed MPNN,[12] attention-MPNN, edge-MPNN and SELU-MPNN.[103] Even the work by Shen W. X. *et al.*[104] who built a convolutional neural network based on a highly customized featurization pipeline including thirteen multidimensional descriptor classes and three fingerprint types was significantly outperformed by our method, a purely SMILES-based model that did not incorporate any topological or structural features directly. Note that the Tox21 dataset listed in this section differs from the original one by Huang R. *et al.*[90] Since the derivative distribution by Wu Z. *et al.*[11] is frequently used for benchmarking, we also trained our CLM on this flavor of Tox21.

In the analysis shown in Table 2, we relied on the data splitting strategy recommended by Wu Z. *et al.*[11] for each dataset. However, splitting molecules randomly between training and testing often results in overly optimistic model performance (due to data collection biases such as limited diversity and sparse coverage of the chemical space). Instead, splitting the scaffolds rather than the molecules poses a more challenging task that might better approximate the generalization performance. We, therefore, re-assessed the performance on three datasets where a random split was recommended

Table 2 ROC-AUC values on the MoleculeNet datasets for different algorithms. With the exception of ClinTox, our method always obtained either the best (bold) or second-best (italic) performance on each dataset. Across all datasets, we outperform all competing approaches. For each dataset, ten models were trained and the splitting strategy recommended by MoleculeNet was utilized

| Dataset	BACE	SIDER	Clintox	BBBP	Tox21	HIV	
Split	Scaffold	Random	Random	Scaffold	Random	Scaffold	Average
Ours (CLM)	$0.861_{\pm 0.04}$	$0.659_{\pm 0.04}$	$0.878_{\pm 0.00}$	$0.915_{\pm 0.02}$	$0.858_{\pm 0.05}$	$0.813_{\pm 0.03}$	**0.831**
GraphConv (Wu Z. et al.)[11]	$0.783_{\pm 0.01}$	$0.638_{\pm 0.01}$	$0.807_{\pm 0.05}$	$0.690_{\pm 0.01}$	$0.829_{\pm 0.01}$	$0.763_{\pm 0.02}$	0.752
Weave (Wu Z. et al.)[11]	$0.806_{\pm 0.00}$	$0.581_{\pm 0.03}$	$0.832_{\pm 0.04}$	$0.671_{\pm 0.01}$	$0.820_{\pm 0.01}$	$0.703_{\pm 0.04}$	0.736
D-MPNN (Yang K. et al.)[12]	$0.838_{\pm 0.06}$	$0.646_{\pm 0.02}$	$\mathbf{0.894_{\pm 0.03}}$	$0.888_{\pm 0.03}$	$0.845_{\pm 0.002}$	$0.794_{\pm 0.02}$	0.818
SELU-MPNN (Withnall M. et al.)[103]	—	$0.632_{\pm 0.01}$	—	$0.693_{\pm 0.06}$	$0.820_{\pm 0.01}$	$0.747_{\pm 0.01}$	—
AMPNN (Withnall M. et al.)[103]	—	$0.639_{\pm 0.01}$	—	$0.709_{\pm 0.04}$	$0.812_{\pm 0.02}$	$0.742_{\pm 0.02}$	—
EMPNN (Withnall M. et al.)[103]	—	$0.651_{\pm 0.01}$	—	$0.705_{\pm 0.02}$	$0.829_{\pm 0.01}$	$0.759_{\pm 0.01}$	—
MMNB (Shen W. X. et al.)[104]	0.849	**0.680**	0.888	0.739	0.842	0.777	0.796
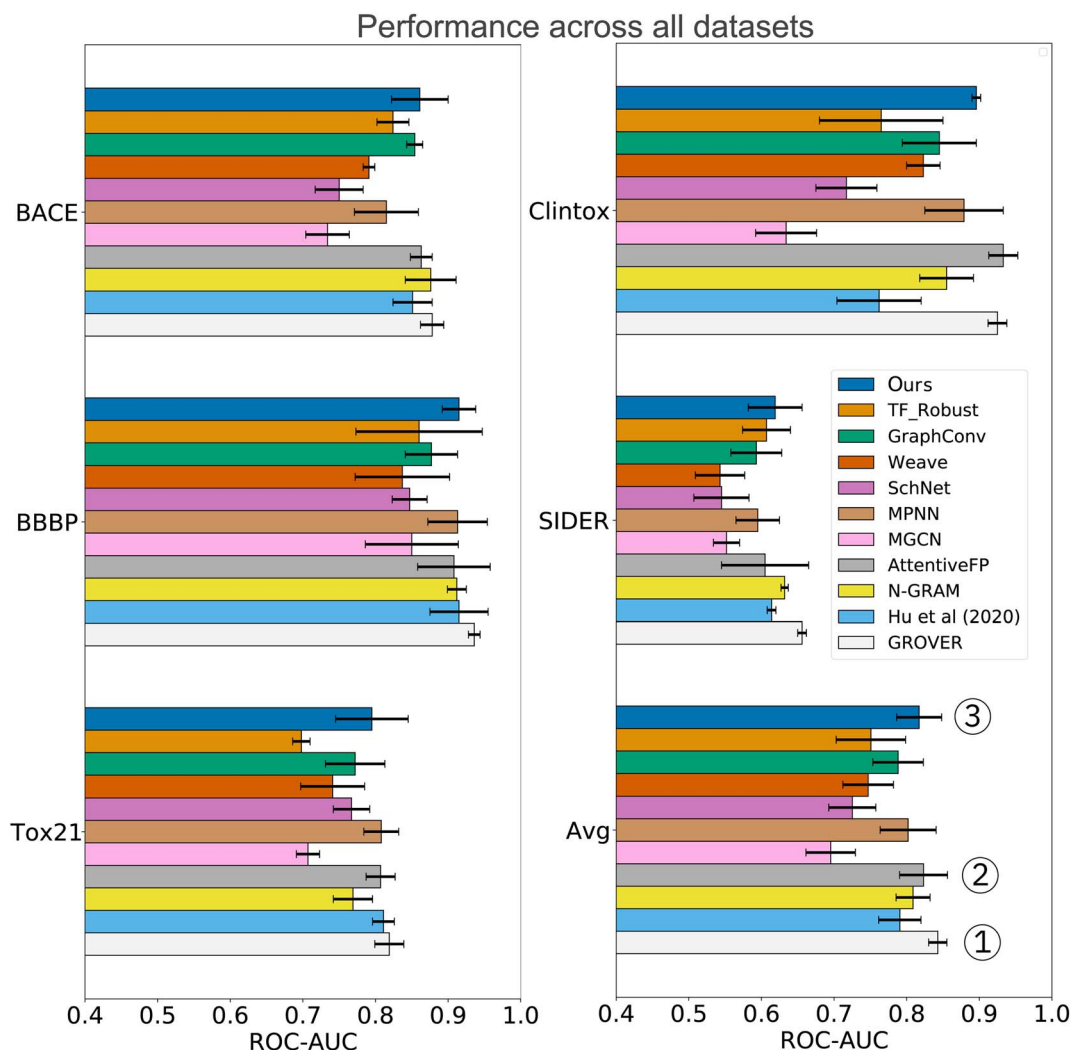
Fig. 4 Comparison to previous work exclusively on scaffold splits of several MoleculeNet datasets. Overall, our CLM is the third best model, only surpassed by GROVER and AttentiveFP. For each dataset, the average ROC-AUC across all tasks is reported. The results were obtained by measuring test performance for 10 repeated scaffold splits. All other numbers are taken from Rong Y. et al.[13] who trained all models on 3 repeated scaffold splits. The detailed numerical results can be found in Table A3, see ESI.‡

(SIDER, ClinTox, and Tox21). The scaffold split on those datasets enabled a fair, yet additional comparison to the benchmarking performed by Rong Y. et al.[13] They evaluated a wide range of prediction models on scaffold splits of all MoleculeNet datasets and then proposed GROVER, a large-scale graph transformer that was pretrained with self-supervision on >10M
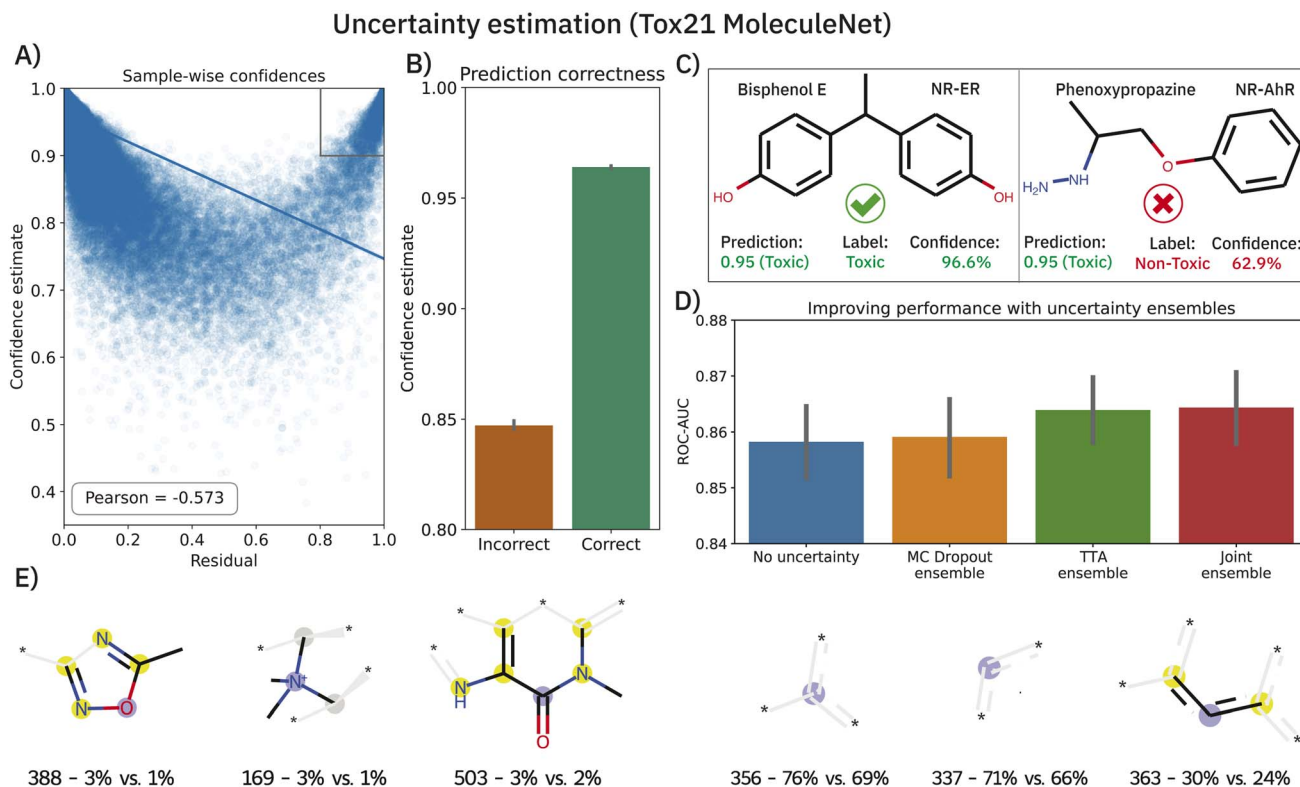
Fig. 5 Uncertainty estimation analysis on the Tox21 MoleculeNet dataset. (A) Scatterplot of prediction residuals and confidences reveals a strong negative correlation. The gray box in the upper right marks molecules that were incorrectly classified with high confidence. (B) Confidence estimates are significantly lower for incorrectly classified samples. (C) Two exemplary molecules, both predicted as toxic, with an incorrect prediction identified from a low confidence estimate. All plots show the results across all 10 splits. (D) The prediction ensembles formed by MC dropout or TTA (test–time data augmentation) can significantly improve the prediction accuracy of the model. (E) The six fragments that were found most predominantly in incorrectly classified high–confidence (ICHC) molecules (see A), gray box. For each fragment, we display the ECFP4 bit and the percentage of ICHC molecules and remaining molecules where this fragment was present. Aromatic atoms are shown in yellow and central atoms in blue.

molecules. The results are displayed in Fig. 4 and include comparisons to fully connected networks (TF_Robust[91]), three graph-convolutional networks (GraphConv,[36] Weave[105] and SchNet[106]), four message-passing graph neural networks (a vanilla GNN[107] and the MPNN[67] and its variants D-MPNN[12] and MGCN[108]), an n-gram model,[109] and two graph transformer networks (AttentiveFP[14] and GROVER itself[13]). The results demonstrate that we consistently obtained superior performance compared to all flavors of fully connected, graph-convolutional or message-passing neural networks. Only the group of graph-transformer networks (AttentiveFP and GROVER) outperformed our model, on average by 0.7% and 3%, respectively. GROVER, the only model that consistently surpasses us, is significantly larger and more complex. Our CLM contains only ~5M parameters (exact number depends on the dataset/vocabulary size), consists of vanilla convolutional layers coupled with plain Bahdanau-style attention, and was trained from scratch on SMILES sequences (with augmentation). AttentiveFP is conceptually similar to our CLM but relies on molecular graphs and graph attention rather than SMILES and sequence attention. Furthermore, AttentiveFP uses recurrent units that are slower than the highly parallelizable convolutions in our model. Note that for AttentiveFP no evidence is given on

the utility of uncertainty estimation techniques to enhance model reliability. Unlike here, their attention analysis only provides qualitative but no quantitative arguments that support model interpretability. Instead, GROVER employs an order of magnitude more parameters ($50M$) and relied on large-scale pretraining on >$11M$ molecules that utilized 250 GPUs.

Lastly, we conducted an ablation study on the impact of the number of heads (m) in the multihead attention. For each $m = 1, 3, 6$ and 12, we computed the area under the ROC curve as the performance measure of the model on four datasets from MoleculeNet,[11] namely, BACE, BBBP, Tox21 and Clintox. Fig. A4, see ESI‡ illustrates the variation in performance of each model across the four datasets. On visualising this performance and the 95% confidence interval associated with it, we conclude that $m = 6$ heads is the best choice in terms of performance and number of parameters to optimise. Please note that we refrained from conducting further ablation studies on the impact of the convolutional or the attention block as a whole because this has been performed in our previously developed PaccMann model [26, Table 1].

3.4 Uncertainty estimation & model ensembling

Deriving prediction confidences is an important topic in chemoinformatics and methods such as nested cross-validation or

snapshot ensembling have been used in the past to understand model trustworthiness.[17,110,111] In this section, we borrow two existing and efficient, yet much simpler methods to estimate model uncertainty in order to assess the reliability of our model's predictions, namely Monte Carlo (MC) dropout[34] and TTA —test-time data augmentation.[35] In both cases, the idea is to obtain a bag of predictions for one molecule (either by dropping out nodes or by passing different SMILES strings corresponding to the same molecule). These experiments were conducted on the Tox21 dataset (MoleculeNet flavor) and the results are shown in Fig. 5. Both—epistemic and aleatoric—model uncertainties were computed for each sample and each of the 12 toxicity assays and subsequently converted into a confidence estimate (*cf.* eqn (6)). Both confidence estimates are strongly negatively correlated with the residual of the prediction: the higher the error, the lower the confidence (Pearson's $r = -0.558$ and -0.536 for epistemic and aleatoric confidence respectively). When averaging both estimates (their correlation is ~0.8), we obtain a single confidence estimate that is even more negatively correlated (see Fig. 5A). While the average confidence is relatively high with a value of 0.94, a known phenomenon,[112] comparing the mean confidences of correctly and incorrectly classified samples reveals significant relative differences (0.96 *versus* 0.85). In a real-world scenario of screening large-scale virtual libraries, this difference could be used out-of-the-box to eliminate molecules where predictions are more likely to be incorrect. A specific example of the benefit of the confidence estimation is shown in Fig. 5C. While Bisphenol E was correctly predicted as toxic for the NR-ER assay, phenoxypropazine was incorrectly predicted as toxic. The model's internal class probabilities are 0.95 in both cases (1 means toxic and 0 non-toxic) and thus do not allow drawing conclusions**. However, investigating the respective prediction confidences (97% *vs.* 63%) can reveal that bisphenol E was a true positive while phenoxypropazine was a false positive.

The scatterplot in Fig. 5A reveals a small subset of incorrectly classified high-confidence (ICHC) molecules (see gray box). These incorrect predictions are particularly undesirable as they cannot be recognized and removed with our method. We inspected the molecules in the gray box (confidence >0.9 and residual >0.8) more closely, aiming to identify fragments that occur commonly in ICHC molecules but rarely in the remaining molecules. In Fig. 5E, we show the six ECFP4 bits that were most indicative for ICHC molecules. In a real-world scenario, such an analysis could easily increase robustness since molecules that include these bits could be removed from the screening library. The three bits shown in Fig. 5E (left) had the highest relative difference between ICHC and the remaining molecules, whereas the three bits shown on the right had the highest absolute difference. Some of these fragments can be linked to tremendous recent literature, for example bit 388 corresponds to a 1,2,4-oxadiazole ring. 1,2,4-Oxadiazole-derivatives have been largely neglected by medicinal chemistry until 2005, but in the past 15 years, research has grown exponentially[113] and only in 2022 researchers reported cytotoxic,[114] fungicidal,[115] anti-

Table 3 Performance on cytotoxicity data. Mean and standard deviations of the test data performance are reported across a 10-fold cross-validation. The best performance for each metric is highlighted in bold. TPR corresponds to sensitivity and TNR to specificity. Bal. Acc. stands for balanced accuracy

Model	Source	Bal. Acc	TPR	TNR
FNN	(Webel HE *et al.*)[30]	$68.89_{\pm 1.46}$	$61.57_{\pm 7.39}$	$76.22_{\pm 6.62}$
Ours	This study	$\mathbf{73.85_{\pm 2.17}}$	$\mathbf{69.81_{\pm 5.82}}$	$\mathbf{77.88_{\pm 5.50}}$

Table 4 Overview of toxic alerts: a subset of 229 alerts, originating from ref. 17, and used for the 17 compounds from the FMP data analysis

Alert class	# alerts	# matches
Genotoxic carcino- & mutagenecity	69	5
Acute aquatic toxicity	54	0
Hepatotoxicity	36	18
Idiosyncratic toxicity	32	9
Mitochondrial toxicity (MT)	17	0
Developmental and MT	12	0
Non-genotoxic carcinogenicity	5	4
Kidney toxicity	4	0

inflammatory,[114] antiparasitary and antiproliferative[116] effects of 1,2,4-oxadiazole derivatives.

The benefits of using MC dropout and TTA are, however, not limited to confidence estimation. The prediction ensembles formed by both methods can be further used to improve the predictions. As demonstrated in Fig. 5D, replacing the baseline predictions (blue), with the mean of the 200 predictions obtained from MC dropout or TTA, improves the ROC-AUC on the Tox21 MoleculeNet benchmark from 0.858 ± 0.001 to 0.859 ± 0.001 (MC dropout) and 0.864 ± 0.001 (TTA). Lastly, a late-fusion average of both techniques yields the best performance (0.865 ± 0.001) which is significantly superior to that of the baseline model across 10 splits ($p < 0.01, W+$). Apart from one unpublished study,[117] this performance is the best-reported one thus far on the highly benchmarked Tox21 dataset.††

3.5 External validation on cytotoxicity data

We validated the performance of our proposed CLM model on an external data set from the FMP.[92] This dataset is comparably large (>34 000 molecules) and indicates for each molecule whether it inhibited relative growth in a kidney and/or a liver cell line by at least 50% (for details see Section 2.6.3). Since this dataset is not generally available to the public, it can serve as an ideal tool to validate our method for potential proprietary use.

3.5.1 Model accuracy. An in-depth study on this large cytotoxicity dataset has been performed by Webel H. E. *et al.*[30] The comparison of their FNN (a fully connected network trained on ECFP4s) to our model is shown in Table 3. Both models achieve good performances on this highly imbalanced cytotoxicity data set. The mean balanced accuracy of the FNN model is

---

** Even though class probabilities are generally insufficient confidence estimators,[34] they are frequently misused in practice for this task.

†† See: **https://paperswithcode.com/sota/drug-discovery-on-tox21**

68.89, whereas we reach a significantly better value (73.85), which is most prominent in the higher sensitivity (TPR). Three major factors that might have induced the better performance of our model are: (1) the use of SMILES sequences has been reported to be superior to that of Morgan fingerprints;[15,26] (2) the use of SMILES augmentation which independently has been shown beneficial[43,118] and (3) the more refined model architecture using an attention mechanism combined with convolution to aggregate local information.

3.5.2 Toxicophore analysis. In the study by Webel H. E. et al.,[30] 17 compounds (7 non-toxic and 10 toxic) from the dataset were selected and published for toxicophore analysis. The same 17 molecules are investigated in this study regarding their attention weights. We extracted known toxicophores (in the form of SMARTS patterns) using 229 substructures from 8 alert classes (see Table 4). This was a subset of the list of 3800 structural alerts from 22 alert classes from the eMolTox server, kindly provided by Ji C. et al.[17] The selection was performed to better represent toxic effects more related to the cytotoxic effects measured in liver (HEPG2) and kidney (HEK292) cells. This led to the exclusion of unspecific alerts, e.g. extended functional groups, PAINS, and others.

From the set of 17 compounds, three case studies are described here, of which the first two are also discussed by Webel H. E. et al.[30] While molecule 1 (Fig. 6A) represents a false negative based on our prediction – a true positive example from Webel H. E. et al.[30] – high attention is attributed to the tertiary substituted ethylendiamine. A similar toxicophore is identified in the study by Webel H. E. et al.[30] and is caught by the given toxicophores from eMolTox,[17] pointing to genotoxic carcinogenicity, mutagenicity, and hepatotoxicity. The second molecule was correctly predicted as cytotoxic ($\hat{y} = 0.96$) and the prediction partly relied on a hepatotoxicity alert from 4-ethylphenol that was also identified by Webel H. E. et al.[30] The third molecule (Fig. 6C) is especially interesting. While it was correctly predicted as toxic by our model and by the FNN from Webel H. E. et al.,[30] both models did not highlight a particularly challenging substructure, namely the thiophene ring, which is sometimes associated with idiosyncratic drug reactions.[17,119] However, the prediction is largely based on the sulfur tail, a hepatotoxicity toxicophore[17] that was not identified by Webel H. E. et al.[30]

Overall, it has to be emphasized that this analysis relied purely on unsupervised learning of toxicophores; neither ours nor the model by Webel H. E. et al.[30] is aware of the notion of toxicophores. While their work mostly focused on the potential identification of new toxicophores, we validated our method in light of existing toxicophores. However, the dark red shaded areas in our attention maps might as well give a good starting point in the search for new toxicophores.

4 Discussion

In this work, we have conducted an extensive comparison of different molecular representations and machine learning models for toxicity and other molecular property prediction. The experiments revealed that competitive performance can be achieved with purely sequence-based chemical language models that do not rely on traditional molecular descriptors (such as fingerprints) or structure-based models (such as graph neural networks). We report evidence that SELFIES,[39] a chemical language devised for generative modeling, exhibits similar predictive power for QSAR tasks as SMILES.

Importantly, we presented a simple and interpretable model that relies solely on SMILES sequences. By coupling our CLM with SMILES augmentation, we surpassed a wide range of previous models and obtained state-of-the-art performance on several QSAR tasks, including but not limited to toxicity. Compared to
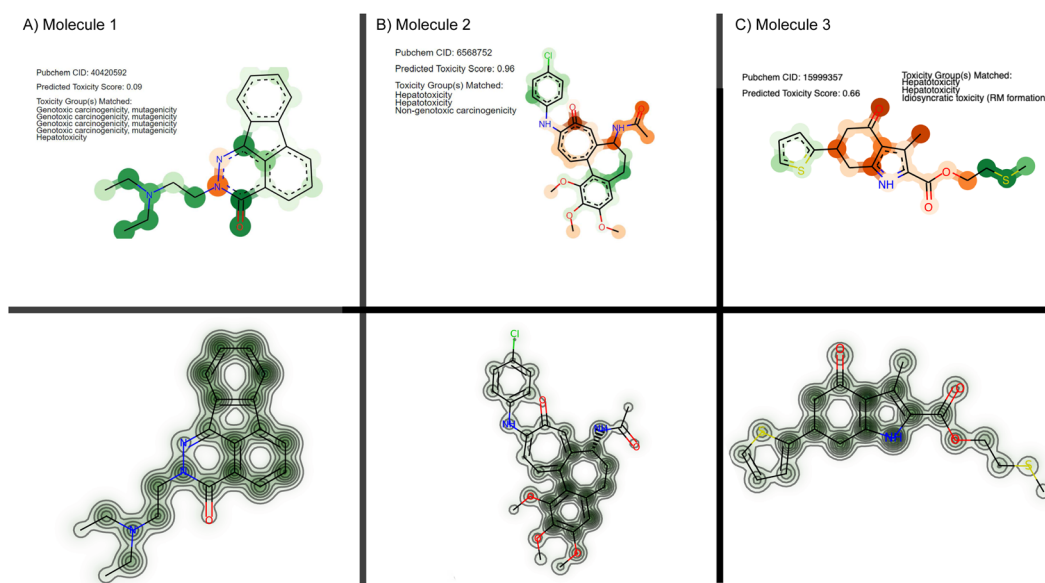

Fig. 6 Cytotoxicity case studies. Three molecules from the FMP dataset are visualized, using either their attention scores from our method (top) or their cytotoxicity maps using deep Taylor decomposition (bottom) following the original work.[30] For our CLM, the color mapping is identical to Fig. 3: green for toxicophore atoms and orange for non-toxicophore atoms. Opacity corresponds to the attention score.

competitive methods, an advantage of our method is that it does not require large-scale pretraining and is thus particularly suitable for low data/resource settings. A key feature of the proposed model is the attention mechanism, an *ante hoc* interpretability method that learns to extract the most important chemical motifs without explicit supervision. On the Tox21 dataset, we demonstrated that the attention on toxicophores is significantly enriched compared to remaining chemical motifs. These attention maps can not only be useful to validate existing toxicophores but also support the identification of so far unknown toxicophores. We validated our CLM on a proprietary toxicity dataset[92] where we consistently outperformed a previous method while enabling similar interpretability analyses. Lastly, we evaluated two simple methods for uncertainty estimation that can not only help to identify misclassified samples but also form an implicit model ensemble that further boosts performance.

In light of the recent success of deep learning in multimodal settings (*e.g.*, chemogenomics and proteochemometrics[120]), future work could explore approaches to featurize toxicity screening assays based on their experimental characteristics. Such models would be even more generic than the multi-task models presented herein because they could be transferred to novel assays and would allow the analysis of the attention scores for a specific assay.

5 Data and code availability

The source code used throughout the work for this paper is available at: **https://github.com/paccmann/toxsmi**. The models trained on the Tox21, SIDER and ClinTox datasets are available in GT4SD,[121] the Generative Toolkit for Scientific Discovery and can be used *via* the properties submodule: **https://github.com/GT4SD/gt4sd-core**. Moreover, these three models are exposed through a Gradio web-app (**https://huggingface.co/spaces/GT4SD/molecular_properties**) where they can be used directly from a UI, either with single SMILES or in batch processing. We released the data preparation and SMILES processing pipeline in a separate PyPI package called pytoda: **https://pypi.org/project/pytoda/**.[46,122] Similarly, the PyTorch implementation for the BRC is available in a separate PyPI package called brc_pytorch: **https://pypi.org/project/brc-pytorch/**.[123] The data from the original Tox21 challenge is available from Huang R. *et al.*:[90] **https://tripod.nih.gov/tox21/challenge/**. The data from the MoleculeNet benchmark is available from Wu Z. *et al.*:[11] **https://moleculenet.org/datasets**. The data from the cytotoxicity case study is available from the FMP authors.[17,92]

Author contributions

Conceptualization: JB, AV, and MM, data curation: JB, GM, and TBK, formal analysis: JB, GM, NJ, and MM, funding acquisition: AV and MRM, investigation: JB, GM, and NJ, methodology: JB, AV, and MM, software: JB, MM, GM, NJ, and TBK, supervision: JB, AV, and MM, validation: JB, NJ, and TBK, visualization: JB, GM, and NJ, writing – original draft: JB, GM, AV, NJ, and TBK, and writing – review and editing: JB, GM, AV, NJ, MRM, and TBK.

	JB	GM	NJ	TBK	AV	MRM	MM
Conceptualization	■				■		■
Data curation	■	■		■			
Formal analysis	■	■	■				■
Funding acquisition					■	■	
Investigation	■	■	■				
Methodology	■				■		■
Software	■	■	■	■			■
Supervision	■				■		■
Validation	■		■	■			
Visualization	■	■	■				
Writing – original draft	■	■	■	■	■		
Writing – review & editing	■	■	■	■	■	■	

Conflicts of interest

The authors declare no conflict of interest.

Acknowledgements

References

1 J. W. Scannell, A. Blanckley, H. Boldon and B. Warrington, Diagnosing the decline in pharmaceutical r&d efficiency, *Nat. Rev. Drug Discovery*, 2012, **11**(3), 191–200.

2 I. Kola and J. Landis, Can the pharmaceutical industry reduce attrition rates?, *Nat. Rev. Drug Discovery*, 2004, **3**(8), 711–716.

3 P. K. Singh, A. Negi, P. K. Gupta, M. Chauhan and R. Kumar, Toxicophore exploration as a screening technology for drug design and discovery: techniques, scope and limitations, *Arch. Toxicol.*, 2016, **90**(8), 1785–1802.

4 E. Lounkine, M. J. Keiser, S. Whitebread, D. Mikhailov, J. Hamon, J. L. Jenkins, *et al.*, Large-scale prediction and testing of drug activity on side-effect targets, *Nature*, 2012, **486**(7403), 361–367.

5 C. H. Wong, K. W. Siah and A. W. Lo, Estimation of clinical trial success rates and related parameters, *Biostatistics*, 2019, **20**(2), 273–286.

6 A. Lin, C. J. Giuliano, A. Palladino, K. M. John, C. Abramowicz, M. L. Yuan, *et al.*, Off-target toxicity is a common mechanism of action of cancer drugs undergoing clinical trials, *Sci Transl Med.*, 2019, **11**(509), eaaw8412.

7 E. Lo.Piparo, A. Worth, *et al.*, *Review of qsar models and software tools for predicting developmental and reproductive toxicity*, JRC Rep EUR, 2010, p. 24522.

8 K. Mansouri, A. Abdelaziz, A. Rybacka, A. Roncaglioni, A. Tropsha, A. Varnek, *et al.*, Cerapp: collaborative estrogen receptor activity prediction project, *Environ. Health Perspect*, 2016, **124**(7), 1023–1033.

9 H. Chen, O. Engkvist, Y. Wang, M. Olivecrona and T. Blaschke, The rise of deep learning in drug discovery, *Drug discovery today*, 2018, **23**(6), 1241–1250.

10 L. Zhang, J. Tan, D. Han and H. Zhu, From machine learning to deep learning: progress in machine intelligence for rational drug discovery, *Drug discovery today*, 2017, **22**(11), 1680–1685.

11 Z. Wu, B. Ramsundar, E. N. Feinberg, J. Gomes, C. Geniesse, A. S. Pappu, *et al.*, Moleculenet: a benchmark for molecular machine learning, *Chem. Sci.*, 2018, **9**(2), 513–530.

12 K. Yang, K. Swanson, W. Jin, C. Coley, P. Eiden, H. Gao, *et al.*, Analyzing learned molecular representations for property prediction, *J. Chem. Inf. Model.*, 2019, **59**(8), 3370–3388.

13 Y. Rong, Y. Bian, T. Xu, W. Xie, Y. Wei, W. Huang, *et al.*, Self-supervised graph transformer on large-scale molecular data, *Advances in Neural Information Processing Systems*, 2020, vol. 33, pp. 12559–12571.

14 Z. Xiong, D. Wang, X. Liu, F. Zhong, X. Wan, X. Li, *et al.*, Pushing the boundaries of molecular representation for drug discovery with the graph attention mechanism, *J. Med. Chem.*, 2019, **63**(16), 8749–8760.

15 T. B. Kimber, M. Gagnebin and A. Volkamer, Maxsmi: maximizing molecular property prediction performance with confidence estimation using smiles augmentation and deep learning, *Artif. Intell. Life Sci.*, 2021, **1**, 100014.

16 A. Mayr, G. Klambauer, T. Unterthiner and S. Hochreiter, Deeptox: toxicity prediction using deep learning, *Front. Environ. Sci.*, 2016, **3**, 80.

17 C. Ji, F. Svensson, A. Zoufir and A. Bender, Emoltox: prediction of molecular toxicity with confidence, *Bioinformatics*, 2018, **34**(14), 2508–2509.

18 H. Yang, L. Sun, W. Li, G. Liu and Y. Tang, In silico prediction of chemical toxicity for drug design using machine learning methods and structural alerts, *Front. Chem.*, 2018, **6**, 30.

19 Y. Peng, Z. Zhang, Q. Jiang, J. Guan and S. Zhou, Top: Towards better toxicity prediction by deep molecular representation learning, in *2019 IEEE International Conference on Bioinformatics and Biomedicine (BIBM)*, IEEE, 2019, pp. 318–325.

20 M. Zaslavskiy, S. Jégou, E. W. Tramel and G. Wainrib, Toxicblend: Virtual screening of toxic compounds with ensemble predictors, *Comput. Toxicol.*, 2019, **10**, 81–88.

21 A. Karim, A. Mishra, M. H. Newton and A. Sattar, Efficient toxicity prediction *via* simple features using shallow neural networks and decision trees, *ACS Omega*, 2019, **4**(1), 1874–1888.

22 K. V. Chuang, L. Gunsalus and M. J. Keiser, Learning molecular representations for medicinal chemistry, *J. Med. Chem.*, 2020, **63**(16), 8705–68722.

23 D. Rogers and M. Hahn, Extended-connectivity fingerprints, *J. Chem. Inf. Model.*, 2010, **50**(5), 742–754.

24 D. Weininger, Smiles, a chemical language and information system 1 introduction to methodology and encoding rules, *J. Chem. Inf. Comput.*, 1988, **28**(1), 31–36.

25 E. N. Muratov, J. Bajorath, R. P. Sheridan, I. V. Tetko, D. Filimonov, V. Poroikov, *et al.*, Qsar without borders, *Chemical Society Reviews*, 2020.

26 M. Manica, A. Oskooei, J. Born, V. Subramanian, J. Saez Rodriguez and M. Rodriguez Martinez, Toward explainable anticancer compound sensitivity prediction *via* multimodal attention-based convolutional encoders, *Mol. Pharm.*, 2019, **16**(12), 4797–4806.

27 N. M. O'Boyle, Towards a universal smiles representation-a standard method to generate canonical smiles based on the inchi, *J. Cheminformatics*, 2012, **4**(1), 22.

28 J. Jiménez Luna, F. Grisoni and G. Schneider, Drug discovery with explainable artificial intelligence, *Nat. Mach. Intell.*, 2020, **2**(10), 573–584.

29 R. P. Sheridan, Interpretation of qsar models by coloring atoms according to changes in predicted activity: how robust is it?, *J. Chem. Inf. Model.*, 2019, **59**(4), 1324–1337.

30 H. E. Webel, T. B. Kimber, S. Radetzki, M. Neuenschwander, M. Nazaré and A. Volkamer, Revealing cytotoxic substructures in molecules using deep learning, *J. Comput.-Aided Mol. Des.*, 2020, **34**(7), 731–746, DOI: 10.1007/s10822-020-00310-4.

31 Q. Ding, S. Hou, S. Zu, Y. Zhang and S. Li, Visar: an interactive tool for dissecting chemical features learned by deep neural network qsar models, *Bioinformatics*, 2020, **36**(11), 3610–3612.

32 J. Jiménez Luna, M. Skalic, N. Weskamp and G. Schneider, Coloring molecules with explainable artificial intelligence for preclinical relevance assessment, *J. Chem. Inf. Model.*, 2021, **61**(3), 1083–1094.

33 D. Bahdanau, K. Cho and Y. Bengio, Neural machine translation by jointly learning to align and translate, in *3rd International Conference on Learning Representations*, ICLR, 2015.

34 Y. Gal and Z. Ghahramani, Dropout as a bayesian approximation: Representing model uncertainty in deep learning, in *International conference on machine learning (ICML)*, PMLR, 2016. pp. 1050–1059.

35 M. S. Ayhan and P. Berens, Test-time data augmentation for estimation of heteroscedastic aleatoric uncertainty in deep neural networks and *Proceedings of the 1st Conference on Medical Imaging with Deep Learning*, MIDL, 2018.

36 T. N. Kipf and M. Welling, Semi-supervised classification with graph convolutional networks, in *J. International Conference on Learning Representations*, ICLR 2017, 2016.

37 H. L. Morgan, The generation of a unique machine description for chemical structures-a technique developed at chemical abstracts service, *J. Chem. Doc.*, 1965, **5**(2), 107–113.

38 T. Le, R. Winter, F. Noé and D. A. Clevert, Neuraldecipher–reverse-engineering extended-connectivity fingerprints (ecfps) to their molecular structures, *Chem. Sci.*, 2020, **11**(38), 10378–10389.

39 M. Krenn, F. Häse, A. Nigam, P. Friederich and A. Aspuru.Guzik, Self-referencing embedded strings

(selfies): A 100% robust molecular string representation, *Mach. Learn.: Sci. Technol.*, 2020, **1**(4), 045024.

40 A. Weber, J. Born and M. Rodriguez Martínez, TITAN: T-cell receptor specificity prediction with bimodal attention networks, *Bioinformatics*, 2021, **37**(Supplement_1), i237–i244, DOI: **10.1093/bioinformatics/btab294**.

41 V. Höll, M. Kouba, M. Dietel and G. Vogt, Stereoisomers of calcium antagonists which differ markedly in their potencies as calcium blockers are equally effective in modulating drug transport by p-glycoprotein, *Biochem. Pharmacol.*, 1992, **43**(12), 2601–2608.

42 G. Landrum, *Rdkit: Open-source cheminformatics, v. 2019', GitHub*, 2019, **https://github.com/rdkit/rdkit**.

43 E. J. Bjerrum, Smiles enumeration as data augmentation for neural network modeling of molecules, *arXiv*, 2017, preprint arXiv:170307076.

44 J. Arús Pous, S. V. Johansson, O. Prykhodko, E. J. Bjerrum, C. Tyrchan, J. L. Reymond, *et al.*, Randomized smiles strings improve the quality of molecular generative models, *J. Cheminformatics*, 2019, **11**(1), 1–13.

45 P. Liu, H. Li, S. Li and K. S. Leung, Improving prediction of phenotypic drug response on cancer cell lines using deep convolutional network, *BMC Bioinf.*, 2019, **20**(1), 408.

46 J. Born, M. Manica, A. Oskooei, J. Cadow, G. Markert and M. R. Martínez, Paccmannrl: De novo generation of hit-like anticancer molecules from transcriptomic data via reinforcement learning, *Iscience*, 2021, **24**(4), 102269.

47 P. Schwaller, T. Gaudin, D. Lanyi, C. Bekas and T. Laino, found in translation": predicting outcomes of complex organic chemistry reactions using neural sequence-to-sequence models, *Chem. Sci.*, 2018, **9**(28), 6091–6098.

48 X. Li and D. Fourches, Smiles pair encoding: A data-driven substructure tokenization algorithm for deep learning, *J. Chem. Inf. Model.*, 2021, **61**(4), 1560–1569.

49 J. Cadow, J. Born, M. Manica, A. Oskooei and M. Rodríguez Martínez, Paccmann: a web service for interpretable anticancer compound sensitivity prediction, *Nucleic Acids Res.*, 2020, **48**(W1), W502–W508.

50 J. Born, Y. Shoshan, T. Huynh, W. D. Cornell, E. J. Martin and M. Manica, On the choice of active site sequences for kinase-ligand affinity prediction, *J. Chem. Inf. Model.*, 2022, **62**(18), 4295–4299, DOI: **10.1021/acs.jcim.2c00840**.

51 J. Born, T. Huynh, A. Stroobants, W. D. Cornell and M. Manica, Active site sequence representations of human kinases outperform full sequence representations for affinity prediction and inhibitor generation: 3d effects in a 1d model, *J. Chem. Inf. Model.*, 2022, **62**(2), 240–257, DOI: **10.1021/acs.jcim.1c00889**.

52 A. Vaswani, N. Shazeer, N. Parmar, J. Uszkoreit, *et al.*, Attention is all you need in *Advances in Neural Information Processing Systems*, 2017. pp. 5998–6008.

53 J. Chung, C. Gulcehre, K. Cho and Y. Bengio, Empirical evaluation of gated recurrent neural networks on sequence modeling, *arXiv*, 2014, preprint arXiv:14123555.

54 N. Vecoven, D. Ernst and G. Drion, A bio-inspired bistable recurrent cell allows for long-lasting memory, *PLoS One*, 2021, **16**(6), e0252676.

55 D. P. Kingma, B. J. Adam, A method for stochastic optimization, in *3rd International Conference on Learning Representations*, ICLR, 2015.

56 L. Breiman: Random forests, *Machine learning*, 2001, vol. 45, pp. 5–32.

57 G. Biau, L. Devroye and G. Lugosi, Consistency of random forests and other averaging classifiers, *J. Mach. Learn. Res.*, 2008, **9**(9).

58 R. L. Marchese Robinson, A. Palczewska, J. Palczewski and N. Kidley, Comparison of the predictive performance and interpretability of random forest and linear models on benchmark data sets, *J. Chem. Inf. Model.*, 2017, **57**(8), 1773–1792.

59 V. Svetnik, A. Liaw, C. Tong, J. C. Culberson, R. P. Sheridan and B. P. Feuston, Random forest: a classification and regression tool for compound classification and qsar modeling, *J. Chem. Inf. Comput. Sci.*, 2003, **43**(6), 1947–1958.

60 T. Tanimoto. An elementary mathematical theory of classification and prediction, ibm report (november, 1958), cited in: G. salton, *automatic information organization and retrieval*, McGraw-Hill New York, 1968.

61 D. K. Duvenaud, D. Maclaurin, J. Iparraguirre, R. Bombarell, T. Hirzel, A. Aspuru.Guzik, *et al.*, Convolutional networks on graphs for learning molecular fingerprints, *Adv. Neural Inf. Process Syst.*, 2015, **28**.

62 S. V. N. Vishwanathan, N. N. Schraudolph, R. Kondor and K. M. Borgwardt, Graph kernels, *J. Mach. Learn. Res.*, 2010, **11**, 1201–1242.

63 K. M. Borgwardt and H. P. Kriegel, Shortest-path kernels on graphs, in *Fifth IEEE International Conference on Data Mining (ICDM'05)*, IEEE, 2005, p. 8.

64 R. W. Floyd, Algorithm 97: shortest path, *Commun. ACM*, 1962, **5**(6), 345.

65 N. Shervashidze, P. Schweitzer, E. J. Van Leeuwen, K. Mehlhorn and K. M. Borgwardt, Weisfeiler-Lehman graph kernels, *J. Mach. Learn. Res.*, 2011, **12**, 2539–2561.

66 G. Nikolentzos and M. Vazirgiannis, Message passing graph kernels, *arXiv*, 2018, preprint arXiv:180802510.

67 J. Gilmer, S. S. Schoenholz, P. F. Riley, O. Vinyals and G. E. Dahl, Neural message passing for quantum chemistry, in *International conference on machine learning*, PMLR, 2017, pp. 1263–1272.

68 M. Togninalli, E. Ghisu, F. Llinares López, B. Rieck and K. Borgwardt: 'Wasserstein weisfeiler-lehman graph kernels', *Advances in Neural Information Processing Systems*, 2019, p. 32.

69 M. A. Hearst, S. T. Dumais, E. Osuna, J. Platt and B. Scholkopf, Support vector machines, *IEEE Intell. Syst.*, 1998, **13**(4), 18–28.

70 J. Kazius, R. McGuire and R. Bursi, Derivation and validation of toxicophores for mutagenicity prediction, *J. Med. Chem.*, 2005, **48**(1), 312–320.

71 Daylight, *Chemical.Information.Systems, I. 'Smarts™—a language for describing molecular patterns*, 2007.

72 N. T. Program, *et al.*, A national toxicology program for the 21st century: A roadmap for the future, National Toxicology Program: Research Triangle Park, NC, USA, 2004.

73 R. R. Tice, C. P. Austin, R. J. Kavlock and J. R. Bucher, Improving the human hazard characterization of chemicals: a tox21 update, *Environ. Health Perspect.*, 2013, **121**(7), 756–765.

74 G. Kerdivel, D. Habauzit and F. Pakdel, *Assessment and molecular actions of endocrine-disrupting chemicals that interfere with estrogen receptor pathways*, 2013.

75 C. Stocco, Tissue physiology and pathology of aromatase, *Steroids*, 2012, **77**(1–2), 27–35.

76 E. Gottlieb, S. Armour, M. Harris and C. Thompson, Mitochondrial membrane potential regulates matrix configuration and cytochrome c release during apoptosis, *Cell Death Differ.*, 2003, **10**(6), 709–717.

77 K. y. Lee, H. Fu, M. I. Aladjem and K. Myung, Atad5 regulates the lifespan of dna replication factories by modulating pcna level on the chromatin, *J. Cell Biol.*, 2013, **200**(1), 31–44.

78 S. Tyagi, P. Gupta, A. S. Saini, C. Kaushal and S. Sharma, The peroxisome proliferator-activated receptor: A family of nuclear receptors role in various diseases, *J. Adv. Pharm. Technol. Res.*, 2011, **2**(4), 236.

79 A. Raghunath, K. Sundarraj, R. Nagarajan, F. Arfuso, J. Bian, A. P. Kumar, *et al.*, Antioxidant response elements: discovery, classes, regulation and potential applications, *Redox Biol.*, 2018, **17**, 297–314.

80 I. A. Murray, A. D. Patterson and G. H. Perdew, Aryl hydrocarbon receptor ligands in cancer: friend and foe, *Nat. Rev. Cancer*, 2014, **14**(12), 801–814. Available from: https://www.nature.com/articles/nrc3846.

81 K. M. Ryan, A. C. Phillips and K. H. Vousden, Regulation and function of the p53 tumor suppressor protein, *Curr. Opin. Cell Biol.*, 2001, **13**(3), 332–337. Available from: http://www.sciencedirect.com/science/article/pii/S0955067400002167.

82 K. Hientz, A. Mohr, D. Bhakta Guha and T. Efferth, The role of p53 in cancer drug resistance and targeted chemotherapy, *Oncotarget*, 2017, **8**(5), 8921.

83 G. Subramanian, B. Ramsundar, V. Pande and R. A. Denny, Computational modeling of β-secretase 1 (bace-1) inhibitors using ligand based approaches, *J. Chem. Inf. Model.*, 2016, **56**(10), 1936–1949.

84 M. Kuhn, I. Letunic, L. J. Jensen and P. Bork, The sider database of drugs and side effects, *Nucleic Acids Res.*, 2016, **44**(D1), D1075–D1079.

85 H. Altae Tran, B. Ramsundar, A. S. Pappu and V. Pande, Low data drug discovery with one-shot learning, *ACS Cent. Sci.*, 2017, **3**(4), 283–293.

86 K. M. Gayvert, N. S. Madhukar and O. Elemento, A data-driven approach to predicting successes and failures of clinical trials, *Cell Chem. Biol.*, 2016, **23**(10), 1294–1301.

87 A. V. Artemov, E. Putin, Q. Vanhaelen, A. Aliper, I. V. Ozerov and A. Zhavoronkov, Integrated deep learned transcriptomic and structure-based predictor of clinical trials outcomes, *BioRxiv*, 2016, p. 095653.

88 I. F. Martins, A. L. Teixeira, L. Pinheiro and A. O. Falcao, A bayesian approach to in silico blood–brain barrier penetration modeling, *J. Chem. Inf. Model.*, 2012, **52**(6), 1686–1697.

89 *Aids antiviral screen data*, 2017. http://wiki.nci.nih.gov/display/NCIDTPdata/AIDS+Antiviral+Screen+Data.

90 R. Huang, M. Xia, D. T. Nguyen, T. Zhao, S. Sakamuru, J. Zhao, *et al.*, Tox21challenge to build predictive models of nuclear receptor and stress response pathways as mediated by exposure to environmental chemicals and drugs, *Frontiers in Environmental Science*, 2016, **3**, 85.

91 B. Ramsundar, P. Eastman, P. Walters and V. Pande, *Deep learning for the life sciences: applying deep learning to genomics, microscopy, drug discovery, and more*, O'Reilly Media, 2019.

92 M. Lisurek, B. Rupp, J. Wichard, M. Neuenschwander, J. P. von Kries, R. Frank, *et al.*, Design of chemical libraries with potentially bioactive molecules applying a maximum common substructure concept, *Mol. Diversity*, 2010, **14**(2), 401–408.

93 L. Bennett, B. Melchers and B. Proppe, *Curta: A general-purpose high-performance computer at ZEDAT*, Freie Universität Berlin'., 2020, DOI: 10.17169/refubium-26754.

94 N. M. Kriege, F. D. Johansson and C. Morris, A survey on graph kernels, *Appl. Netw. Sci.*, 2020, **5**(1), 1–42.

95 H. J. M. Verhaar, C. J. van Leeuwen and J. L. M. Hermens, Classifying environmental pollutants, *Chemosphere*, 1992, **25**(4), 471–491.

96 J. L. M. Hermens, Electrophiles and acute toxicity to fish, *Environ. Health Perspect.*, 1990, **87**, 219–225.

97 M. Nendza, A. Wenzel, M. Müller, G. Lewin, N. Simetska, F. Stock, *et al.*, Screening for potential endocrine disruptors in fish: evidence from structural alerts and in vitro and in vivo toxicological assays, *Environ. Sci. Eur.*, 2016, **28**(1), 26. Available from: http://enveurope.springeropen.com/articles/10.1186/s12302-016-0094-5.

98 I. Sushko, E. Salmina, V. A. Potemkin, G. Poda and I. V. Tetko, Toxalerts: a web server of structural alerts for toxic chemicals and compounds with potential adverse reactions, *J. Chem. Inf. Model.*, 2012, **52**(8), 2310–2316.

99 M. Karimi, D. Wu, Z. Wang and Y. Shen, Deepaffinity: interpretable deep learning of compound–protein affinity through unified recurrent and convolutional neural networks, *Bioinformatics*, 2019, **35**(18), 3329–3338.

100 M. Tsubaki, K. Tomii and J. Sese, Compound–protein interaction prediction with end-to-end learning of neural networks for graphs and sequences, *Bioinformatics*, 2019, **35**(2), 309–318.

101 S. Li, F. Wan, H. Shu, T. Jiang, D. Zhao and J. Zeng, Monn: a multi-objective neural network for predicting compound-protein interactions and affinities, *Cell Syst.*, 2020, **10**(4), 308–322.

102 K. Preuer, G. Klambauer, F. Rippmann, S. Hochreiter and T. Unterthiner, 'Interpretable deep learning in drug discovery', Explainable AI: interpreting, explaining and visualizing deep learning, 2019, pp. 331–345.

103 M. Withnall, E. Lindelöf, O. Engkvist and H. Chen, Building attention and edge message passing neural networks for

bioactivity and physical–chemical property prediction, *J. Cheminformatics*, 2020, **12**(1), 1–18.

104 W. X. Shen, X. Zeng, F. Zhu, C. Qin, Y. Tan, Y. Y. Jiang, *et al.*, Out-of-the-box deep learning prediction of pharmaceutical properties by broadly learned knowledge-based molecular representations, *Nat. Mach. Intell.*, 2021, **3**(4), 334–343.

105 S. Kearnes, K. McCloskey, M. Berndl, V. Pande and P. Riley, Molecular graph convolutions: moving beyond fingerprints, *J. Comput.-Aided Mol. Des.*, 2016, **30**(8), 595–608.

106 K. Schütt, P. J. Kindermans, H. E. Sauceda Felix, S. Chmiela, A. Tkatchenko and K. R. Müller, Schnet: A continuous-filter convolutional neural network for modeling quantum interactions, *Adv. Neural Inf. Process Syst.*, 2017, **30**.

107 W. Hu, B. Liu, J. Gomes, M. Zitnik, P. Liang, V. S. Pande, *et al.*, Strategies for pre-training graph neural networks, *8th International Conference on Learning Representations*, ICLR 2020, 2020.

108 C. Lu, Q. Liu, C. Wang, Z. Huang, P. Lin and L. He Molecular property prediction: A multilevel quantum interactions modeling perspective, in *Proceedings of the AAAI Conference on Artificial Intelligence*, 2019, vol. 33, pp. 1052–1060.

109 S. Liu, M. F. Demirel and Y. Liang, N-gram graph: Simple unsupervised representation for graphs, with applications to molecules, *Adv. Neural Inf. Process Syst.*, 2019, **32**.

110 D. Baumann and K. Baumann, Reliable estimation of prediction errors for qsar models under model uncertainty using double cross-validation, *J. Cheminformatics*, 2014, **6**(1), 1–19.

111 I. Cortés Ciriano and A. Bender, Deep confidence: a computationally efficient framework for calculating reliable prediction errors for deep neural networks, *J. Chem. Inf. Model.*, 2018, **59**(3), 1269–1281.

112 C. Corbiere, N. Thome, A. Saporta, T. H. Vu, M. Cord and P. Perez, Confidence estimation via auxiliary models, *IEEE Trans. Pattern Anal. Mach. Intell.*, 2021.

113 T. M. Dhameliya, S. J. Chudasma, T. M. Patel and B. P. Dave, A review on synthetic account of 1, 2, 4-oxadiazoles as anti-infective agents, *Mol. Diversity*, 2022, 1–14.

114 B. Ruan, X. Tang, W. Guo, Y. Hu and L. Chen, Synthesis and biological evaluation of novel phthalide analogs-1, 2, 4-oxadiazole hybrids as potential anti-inflammatory agents, *Chem. Biodiversity*, 2022, **19**(8), e202200039.

115 B. L. Sun, Y. Y. Wang, S. Yang, M. T. Tu, Y. Y. Shao, Y. Hua, *et al.*, Benzamides substituted with quinoline-linked 1, 2, 4-oxadiazole: Synthesis, biological activity and toxicity to zebrafish embryo, *Molecules*, 2022, **27**(12), 3946.

116 Y. M. Rocha, E. P. Magalhães, M. de Medeiros Chaves, M. Machado Marinho, V. Nascimento e Melo de Oliveira, R. Nascimento de Oliveira, *et al.*, Antiparasitary and antiproliferative activities in vitro of a 1, 2, 4-oxadiazole derivative on trypanosoma cruzi, *Parasitol. Res.*, 2022, 1–16.

117 Z. Alperstein, A. Cherkasov and J. T. Rolfe, All smiles variational autoencoder, *arXiv*, 2019, preprint arXiv:190513343.

118 I. V. Tetko, P. Karpov, E. Bruno, T. B. Kimber and G. Godin Augmentation is what you need!, in *International Conference on Artificial Neural Networks*, Springer, 2019, pp. 831–835.

119 N. L. Dang, T. B. Hughes, G. P. Miller and S. J. Swamidass, Computational approach to structural alerts: furans, phenols, nitroaromatics, and thiophenes, *Chem. Res. Toxicol.*, 2017, **30**(4), 1046–1059.

120 B. J. Bongers, A. P. IJzerman and G. J. Van.Westen: '*Proteochemometrics–recent developments in bioactivity and selectivity modeling*', Drug Discovery Today: Technologies, 2020.

121 M. Manica, J. Cadow, D. Christofidellis, A. Dave, J. Born, D. Clarke, *et al.*, Gt4sd: Generative toolkit for scientific discovery, *NPJ Computational Materials*, in press.

122 J. Born, M. Manica, J. Cadow, G. Markert, N. A. Mill, M. Filipavicius, *et al.*, Data-driven molecular design for discovery and synthesis of novel ligands: a case study on SARS-CoV-2, *Mach. Learn.: Sci. Technol.*, 2021, **2**(2), 025024. Available from: **https://iopscience.iop.org/article/10.1088/2632-2153/abe808**.

123 N. Janakarajan, J. Born, M. Manica, A fully differentiable set autoencoder, in *Proceedings of the 28th ACM SIGKDD Conference on Knowledge Discovery and Data Mining. KDD '22.*, Association for Computing Machinery, New York, NY, USA, 2022. pp. 3061–3071. DOI: **10.1145/3534678.3539153**.

124 B. Rieck, *Latex-credits, BSD-3-Clause*, **https://github.com/Pseudomanifold/latex-credits**.